NASA TECHNICAL REPORT

NASA TR R-236

NASA TR R-236

MINIMIZATION OF THE TOTAL HEAT INPUT FOR MANNED VEHICLES ENTERING THE EARTH'S ATMOSPHERE AT HYPERBOLIC SPEEDS

by Alvin Seiff and Michael E. Tauber

Ames Research Center
Moffett Field, Calif.

NATIONAL AERONAUTICS AND SPACE ADMINISTRATION - WASHINGTON, D. C. - MAY 1966

NASA TR R-236

MINIMIZATION OF THE TOTAL HEAT INPUT FOR MANNED VEHICLES ENTERING THE EARTH'S ATMOSPHERE AT HYPERBOLIC SPEEDS

By Alvin Seiff and Michael E. Tauber

Ames Research Center
Moffett Field, Calif.

NATIONAL AERONAUTICS AND SPACE ADMINISTRATION

For sale by the Clearinghouse for Federal Scientific and Technical Information
Springfield, Virginia 22151 – Price $3.00

TABLE OF CONTENTS

MINIMIZATION OF THE TOTAL HEAT INPUT FOR MANNED VEHICLES ENTERING THE EARTH'S ATMOSPHERE AT HYPERBOLIC SPEEDS

By Alvin Seiff and Michael E. Tauber
Ames Research Center

SUMMARY

The use of conical entry bodies to control the radiative and minimize the total heat input to manned vehicles is investigated with an imposed acceleration limit on two types of hyperbolic shallow-angle entry into the Earth's atmosphere. The local Reynolds number is limited to retain laminar boundary layer. The equations permit any desired values of the acceleration and local Reynolds number limits and of the body radius, body density, and heat-shield material properties. Numerical examples are given for a range of Reynolds number limits, three body radii, and two heat-shield materials.

The dependences of the convective and radiative heating rates on air density, velocity, cone angle, and base radius are written and integrated over the trajectory in an expression which is particularly simple for nearly horizontal flight. The major reduction in convective heating due to transpiration from the heat shield is included, although somewhat uncertainly for the higher speeds. The heat inputs are expressed as fractions of the vehicle kinetic energy at entry to obtain a dimensionless figure of merit for comparing cases of different vehicle mass or entry velocity. Trajectories analyzed include constant altitude deceleration and constant Reynolds number descent. The latter is the trajectory of minimum convective heat input for a given Reynolds number limit, and of minimum total heat input in cases where the radiative contribution is small. Aerodynamic lift required to follow these trajectories is discussed.

For any specified set of entry conditions, the cone angle has an optimum value which diminishes with increasing entry velocity. The optimum cones generally have small total radiative heat input compared to convective. For cone angles larger than optimum, the radiative and total heat inputs can become many times greater than the optimum. The total heat input energy fraction is a sensitive function of body size on acceleration-limited entries. It is smallest for large bodies of the order of 3- to 4-meters base radius - for example, less than 1 percent of kinetic energy at entry for velocities up to about 24 km/sec. The corresponding mass loss may be less than 20 percent of total mass at entry. With small bodies or very low Reynolds number limits, the optimum energy fraction is increased several fold. While the heating may be manageable, the requirements for lift-drag ratio and acceleration limiting appear to become difficult to satisfy aerodynamically with optimum cones on a single pass at entry velocities above about 25 km/sec.

INTRODUCTION

As space flight missions go to progressively greater distances from the earth, the speed of entry into the atmosphere on return to earth tends to increase. Thus, intercontinental ballistic vehicles and near-earth satellites enter the atmosphere at 6 to 8 km/s; returning lunar vehicles, at 11 km/s; and vehicles returning from the near planets, at speeds as high as 20 km/s. Still higher entry speeds are likely to arise in connection with future missions not yet considered in detail.

At the lower speeds, the entry heating has been readily controlled by the use of configurations which direct most of the vehicle kinetic energy into heating the atmosphere (ref. 1), and by the use of ablation shields which block and absorb the energy converted to heat in the boundary layer. However, the total energy to be dissipated (per unit of vehicle mass) increases with the square of entry velocity, and, as will be shown, the fraction of the vehicle kinetic energy deposited as heat in the body also tends to increase with entry velocity. Successful solution of the heating problem at high entry velocities depends on maintaining this heating energy fraction small.

The principal mechanism for body heating at velocities less than 10 km/s is boundary-layer convection. At higher velocities, the gas in the shock layer may attain temperatures well in excess of 10,000° K and radiate substantial amounts of energy at optical and ultraviolet wavelengths (ref. 2). This radiation falling on the body tends to become the predominant heating mechanism for blunt bodies and increases the fraction of the vehicle energy converted to body heat input.

While the intensity of radiative heating at any wavelength cannot exceed that of a black body at the temperature of the shock layer and, for some low altitude flight conditions, may approach that limit, such heating rates would generally be considered unacceptably large. For example, at the modest shock-layer temperature of 6500° K, the black body intensity is 10^5 kW/m^2. Heating rates are also limited by the energy available in the incident flow. For the portion of the trajectory where the deceleration is large, the available flow energy is also large ($(1/2)\rho V^3 A = ma_x\ V/C_D$), and substantial fractions of it can be radiated toward the body. Thus, these two limiting effects do not prevent the radiative heating from assuming very large values.

It has been shown in references 3 through 6 that radiative intensity is reduced for bodies, such as cones, which have oblique bow shock waves. As is well known, the oblique shock wave is equivalent to a normal shock wave at the lower flight velocity $U = V \sin \theta_w$. Furthermore, the radiative emission behind a normal shock wave varies as a high power of the velocity (refs. 2 and 5) so that sweepback of the shock wave offers a powerful means of reducing radiative input. Bodies having oblique shock waves, however, exhibit smaller drag coefficients than blunt bodies, and this results in increased convective heat input, as will be shown. Therefore, an optimum cone angle will be found which minimizes the sum of convective and radiative inputs. The analysis of reference 5 defines these optima for ballistic entry. It was found that the fraction of entry kinetic energy that enters the body as heat may be kept

below 0.01 at optimum for entry velocities to 30 km/s, if the trajectory is limited to a peak Reynolds number below the transition Reynolds number. It follows that such high-speed entries might be made with a relatively small heat-shield mass loss.

The vehicle accelerations on ballistic entry at such velocities are large, hundreds to thousands of times the earth's gravitational acceleration, and are far in excess of human tolerance. The question of optimum bodies for manned entry at hyperbolic speeds therefore remains to be treated and is the present subject. The restriction to suitably low levels of acceleration is obtained by choice of trajectories of shallow angle, sometimes called grazing trajectories. Two kinds of grazing trajectories are treated - constant altitude decelerations and constant Reynolds number descents. The limitation imposed on entry by the lift required at supercircular speeds is considered. Optimum cone angles are defined, and the fractions of entry kinetic energy that go into heating the body are calculated. Simplifying assumptions are made, so as to obtain generality, and a range of entry parameters is considered. The heating analysis follows that of reference 5. The problem of ablating the tip during entry is analyzed to determine if an effectively sharp conical body can be maintained.

Preliminary results of the analysis have been given in references 7, 8, and 9.

NOTATION

a entry vehicle acceleration, m/s^2

$\underline{a}$ shock-wave area, m^2

A body frontal area, m^2

B ballistic parameter, $C_D \rho_o A/\beta m \sin \gamma_E$

c_p gas specific heat at constant pressure, J/kg ^oK

C_c laminar convective constant (eq. (17)), $(s/m)^j m^{0.5}$

C_D drag coefficient, dimensionless

C_e equilibrium radiative constant (eq. (10)), $(W/m^3)(s/m)^q$

C_H heat-transfer coefficient, dimensionless

C_n nonequilibrium radiative constant (eq. (13)), $(W/m^2)(s/m)^s$

D drag force, N

$\dot{E}$	power radiated from gas in shock layer, W
F	convective heating correlation constant (eq. (A1)), $(m/s)^{0.36}$
g	acceleration due to gravity, m/s^2
h	local static enthalpy, J/kg
h_t	streamline total enthalpy, J/kg
H	heat input integrated over body and over time, J
i	defined in equation (13)
I	laminar convective heating integral (eq. (29)), $(m/s)^{j+2}$
j	velocity exponent (eq. (16))
k	constant (eq. (35))
K	ρV, a constant on constant Reynolds number trajectories, kg/m^2s
K_c	α/ζ, $(s/m)^2$
L	lift force, N
m	entry vehicle mass, kg
Nu	Nusselt number (eq. (A2))
p	density exponent (eq. (10))
p_w	cone surface pressure, N/m^2
q	velocity exponent (eq. (10))
$\underline{q}$	local laminar convective heating rate (eq. (A2)), W/m^2
q_∞	free-stream dynamic pressure, appendix C, N/m^2
r_b	body base radius, m
r_n	body nose radius, m
R	gas constant, J/kg ^oK
Re	Reynolds number based on base radius and free-stream air properties
Re_ϵ	Reynolds number based on slant length and properties at boundary-layer edge

Re_l maximum allowable value of Re_ϵ

R_p radius of planet, m

s velocity exponent (eq. (13))

S slant length of cone

t time, s

T temperature, ^oK

u air velocity in the shock layer, relative to the body, m/s

U component of flight velocity normal to shock wave, m/s

$U_{1,2}$ velocity of change in the equilibrium radiative constants, 13,700 m/s

v volume, m^3

V flight velocity, m/s

V_s near-earth satellite velocity, 7900 m/s

W entry vehicle weight, N

x range measured along flight path, m

$\dot{x}_n$ rate of axial regression of the tip due to ablation, m/s

y altitude, m

Z moles per original mole

α transpiration effectiveness parameter

α_t trim angle of attack

β reciprocal of atmospheric scale height (eq. (C18)), m^{-1}

γ flight-path angle below horizontal

δ shock-wave standoff distance (eq. (E4)), m

ζ energy to ablate unit mass of heat shield, J/kg

η $\frac{H}{mV_E^2/2}$, dimensionless

θ_c cone half-angle

θ_w	conical bow wave half-angle
μ	gas viscosity, kg/m·s
ρ	air density, kg/m^3
$\overline{\rho}$	ρ/ρ_o
ρ_b	body density, kg/m^3
σ	value of ψ for $V \to \infty$ (eq. (18))
ψ	$C_{H_c}/C_{H_{c_o}}$
$(\dot{})$	derivative with respect to time

Subscripts

c	laminar convective
c_l	collision limiting
c_o	laminar convective in absence of ablation
e	equilibrium radiative
E	at entry into the atmosphere
l	limiting or maximum permissible value
min	minimum
n	nonequilibrium radiative
o	earth sea-level condition
opt	optimum
st	stagnation point
w	evaluated at vehicle surface
x	horizontal component, or component along the flight path
y	vertical component, or component normal to flight path
ϵ	evaluated at boundary-layer edge
2	shock-layer properties

Stream properties without subscript are evaluated in the free stream.

ANALYSIS

Heating Equations

The rate of heat energy input to a vehicle flying in the atmosphere may be expressed as a fraction C_H of the kinetic energy $\rho V^3 A/2$ of the air intercepting the body per unit time

$$\frac{dH}{dt} = C_H \frac{\rho V^3 A}{2} \tag{1}$$

To satisfy the conservation of energy, the heat-transfer coefficient C_H defined by equation (1) cannot exceed 1.0. The work converted to heat by the total drag force per unit time

$$DV = C_D \frac{\rho V^3 A}{2} \tag{2}$$

results partly in heating the atmosphere and partly in heating the entry vehicle. That is, $dH/dt < DV$, so that C_H/C_D is less than 1 and represents the fraction of the work done by the drag force which goes into heating the vehicle.

The total heat input on a trajectory is obtained by integrating equation (1)

$$H = \int_0^{t_{V=0}} C_H \frac{\rho V^3 A}{2} \, dt \tag{3}$$

Equation (3) is evaluated in reference 5 for rectilinear ballistic entry into an exponential atmosphere. For other trajectories, it can be integrated if the dependence of C_H, ρ, and V on t is established. Since C_H can be expressed as a complicated function of ρ, V, and r_b for a given body shape, relations between ρ, V, and t which permit the expression of the integral in terms of one variable are sought. These relations are provided by the trajectory equations.

The rate of velocity change along the flight path may be written

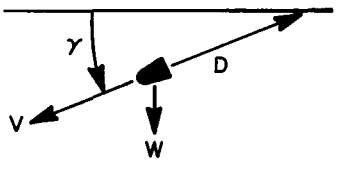

Sketch (a)

$$-m \frac{dV}{dt} = C_D \frac{\rho V^2 A}{2} - mg \sin \gamma \tag{4}$$

For trajectories within the atmosphere, with the drag force comparable to or larger than the weight, and at small values of γ, this becomes, very closely,

$$-m \frac{dV}{dt} = C_D \frac{\rho V^2 A}{2}$$

from which

$$dt = - \frac{m}{C_D A} \frac{2}{\rho} \frac{dV}{V^2} \tag{5}$$

Thus, for flight at or near zero path angle γ, equation (3) becomes

$$H = \int_0^{V_E} \frac{C_H}{C_D} mV \, dV \tag{6}$$

which depends on ρ only through the dependence of C_H on ρ. For reference, it is informative to consider the case C_H/C_D = constant. Then, with constant vehicle mass, equation (6) may be integrated to obtain $H = (C_H/C_D)(mV_E^2/2)$. Here, C_H/C_D is seen to be the fraction of kinetic energy at entry which is converted to body heat. With C_H variable, the total heat input H may still be expressed as a fraction η of the kinetic energy of the vehicle at entry

$$H = \frac{\eta(mV_E^2)}{2} \tag{7}$$

where η is a weighted mean value of C_H/C_D, defined by combining equations (6) and (7) to obtain, for a constant vehicle mass,

$$\eta = 2 \int_0^1 \frac{C_H}{C_D} \frac{V}{V_E} \, d \frac{V}{V_E} \tag{8}$$

It is seen that η may be made small by minimizing the area under the curve $(C_H/C_D)V$ as a function of V. Note that equations (7) and (8) show that the total heat input is inversely proportional to drag coefficient.

The mass lost by ablation may be written, for cases where the heat stored is small compared to that resulting in ablation,

$$\frac{\Delta m}{m_E} = \frac{\eta V_E^2}{2\zeta} \tag{9}$$

where ζ is the energy absorbed per unit mass of material ablated.

The Heat-Transfer Coefficient

The heat-transfer coefficient C_H is a function of the flight velocity, stream density, body shape and size, atmospheric composition, and nature of the boundary layer. Even when the boundary layer is laminar, the heat transferred by convection at the speeds considered is very large; while with a turbulent boundary layer, the convective heat input integrated over the trajectory is from 5 to 10 times larger (ref. 5). The present analysis seeks to define conditions of minimum total heat input, and these will clearly correspond to those which maintain a laminar boundary layer. It is assumed that laminar flow can be maintained by restricting the local Reynolds number below

some specified limit. The appropriate critical value or values for this limit are presently unknown for conditions of high total enthalpy flow over an ablating surface. Therefore, the value to be chosen is treated as a parameter of the analysis, and the analysis is restricted to a consideration of the laminar flow boundary layers.

The heat-transfer coefficient is necessarily treated in three parts, the laminar convective contribution, C_{H_c}, the equilibrium radiative contribution, C_{H_e}, and the nonequilibrium radiative contribution, C_{H_n}. The latter two are assumed to be given by equations from reference 5, reproduced below.

The radiative power emitted per unit of shock-layer volume at equilibrium is

$$\frac{d\dot{E}}{dv} = C_e U^q \bar{\rho}^p \tag{10}$$

where $U = V \sin \theta_w$ is the component of velocity normal to the shock wave and $\bar{\rho} = \rho/\rho_o$. Values of the constant and exponents are, for air,

$$\left.\begin{aligned} C_{e_1} &= \frac{6.14}{10^{49}} \frac{W}{m^3} \left(\frac{s}{m}\right)^{15.45} \\ q_1 &= 15.45 \\ p &= 1.80 \end{aligned}\right\} \quad U < 13{,}700 \text{ m/s} \tag{11a}$$

and

$$\left.\begin{aligned} C_{e_2} &= \frac{6.44}{10^{6}} \frac{W}{m^3} \left(\frac{s}{m}\right)^{5.05} \\ q_2 &= 5.05 \\ p &= 1.80 \end{aligned}\right\} \quad U > 13{,}700 \text{ m/s} \tag{11b}$$

with $\rho_o = 1.225$ kg/m^3. The equilibrium radiative component of C_H may be written

$$C_{H_e} = C_e V^{(q-3)} \bar{\rho}^{(p-1)} \frac{r_b}{\rho_o} \frac{\tan^2 \theta_w - \tan^2 \theta_c}{3 \tan^3 \theta_c} (\sin \theta_w)^q \tag{12}$$[1]

Values of the wave angle θ_w for cones in high velocity flow are given in figures 35 and 36 of reference 5, based on the analysis in appendix B of that reference.

---

[1]For considering the dimensional consistency of equation (12), note that in the mks system the W/m^3 is identical to the mechanical unit kg/(m)s^3. Similarly, in equations (13), (14), and (15) the W/m^2 is identical to the kg/s^3.

The nonequilibrium radiative power unit of shock-wave surface is assumed, following arguments given in reference 2, for example, to be a function of the velocity U only, above a certain ambient density, ρ_{cl}

$$\frac{d\dot{F}}{da} = C_n U^s \left(\frac{\bar{\rho}}{\bar{\rho}_{cl}}\right)^i \tag{13}$$

where

$$C_n = \frac{1.15}{10^{11}} \frac{W}{m^2} \left(\frac{s}{m}\right)^{4.1} , \quad s = 4.1 \tag{14}$$

and we have used $\bar{\rho}_{cl} = 10^{-3}$ as in reference 5.

In the "collision limited" regime $i = 1$, while for $\rho > \rho_{cl}$, $i = 0$, and the nonequilibrium component of the heat-transfer coefficient which follows from this is

$$C_{H_n} = C_n \frac{V^{s-3}}{\rho} \left(\frac{\tan \theta_w}{\tan \theta_c}\right)^2 (\sin \theta_w)^{s-1} \left(\frac{\bar{\rho}}{\bar{\rho}_{cl}}\right)^i \tag{15}$$

The convective heat-transfer coefficient may be written, based on a recent analysis of equilibrium real air boundary-layer heat transfer to pointed cones (ref. 10),

$$C_{H_{co}} = \frac{C_c V^j}{\sqrt{r_b \bar{\rho}}} \sqrt{\sin 2\theta_c} \tag{16}$$

with

$$C_c = \frac{0.84}{10^4} \left(\frac{s}{m}\right)^{1/6} m^{0.5} \tag{17}$$

$$j = 1/6$$

It will be noted that this coefficient and exponent differ from those given in reference 5. Appendix A derives equations (16) and (17) from the correlation given in reference 10, and compares the values of $C_{H_{co}}$ with those of reference 5.[2]

The convective heat transfer in the presence of ablation is reduced by the transpiration cooling effect of the ablation vapors. Following reference 5 we assume

$$\Psi = \frac{C_{H_c}}{C_{H_{co}}} = \frac{1 - \sigma}{1 + K_c V^2} + \sigma \tag{18}$$

---

[2]Values of C_c and j derived in appendix A for $T_w = 3000^\circ$ K, and p_w between 0.1 and 1.0 atmosphere are 1.16×10^{-4} and 0.14, respectively. For velocities between 10 and 20 km/s, values of $C_{H_{co}}$ given by these constants and those of equation (17) differ by less than 5 percent. The choice of $j = 1/6$ is advantageous because it permits integration of the convective heating over the trajectory in closed form, as will be shown.

where $K_c = \sigma/\zeta$, α is a laminar transpiration effectiveness parameter that depends on the molecular weight of the ablation products (ref. 11), ζ is the energy per unit mass (mechanical energy units) required to heat, dissociate, and vaporize the ablation material, and σ is an assumed asymptotic value of $C_{H_c}/C_{H_{c_o}}$ for infinite velocity.

With $\sigma = 0$, equation (18) gives $\psi = 0$ at infinite velocity. This corresponds to infinite effective heat of ablation (a concept not used herein) at infinite total enthalpy. Provision of the term σ as an asymptotic limit of ψ for $V \to \infty$ is based on experimental results from Ames Research Center arc jet facilities (ref. 12) which suggest that the factor ψ does not go to zero but to a small fractional value of the order of 0.1. Since the behavior of ablation shields at the high velocities considered here is not well established, the effect of varying the asymptote σ from 0 to 0.1 will be shown.

It may also be remarked that for charring organic ablators, the true heat of ablation ζ is not a constant, being a function of the degree of dissociation of the gaseous products and, therefore, of the temperature of the ablating surface. Hence, it depends on the heat-transfer rate and distribution between the convective and radiative contributions. Since the study of such materials is quite specific to the material chosen and too complicated for parametric treatment, it was not attempted here. The materials chosen for the examples were a low temperature organic ablator, Teflon, and a material with a large heat of vaporization, quartz, which is assumed to vaporize and not run off the surface as a liquid. (In practice, quartz does suffer liquid runoff, particularly at moderate heating rates.) The choice of these materials is intended to be illustrative, and does not imply a judgment by the authors that they represent leading contending materials for high speed entry. A third material, graphite, was included because it appeared to offer advantages for protection of the conical tip. The assumed properties of these materials are given in the following table.

	α	ζ, $(m/s)^2$	K_c, $(s/m)^2$
Teflon	0.26	2.2×10^6	12.0×10^{-8}
Quartz	0.24	16.0×10^6	1.5×10^{-8}
Graphite	0.42	67.0×10^6	0.63×10^{-8}

For comparison, the heat of ablation ζ of the charring ablator, phenolic nylon, at a high surface temperature, 3500° K, has been estimated to be as high as 28×10^6 $(m/s)^2$ (ref. 13). Thus, its mass losses, exclusive of chemical and mechanical erosion, should be somewhat smaller than those of vaporizing quartz as presented herein. For graphite, α is again chosen to follow the molecular weight dependence suggested in reference 11, and the heat of ablation is taken from data in reference 14.

Integration of the Heat-Transfer Equation

In terms of the components of heat input, $C_H = C_{H_c} + C_{H_e} + C_{H_n}$, equation (8) becomes

$$\eta = 2\int_o^1 \frac{C_{H_c}}{C_D}\frac{V}{V_E}\,d\,\frac{V}{V_E} + 2\int_o^1 \frac{C_{H_e}}{C_D}\frac{V}{V_E}\,d\,\frac{V}{V_E} + 2\int_o^1 \frac{C_{H_n}}{C_D}\frac{V}{V_E}\,d\,\frac{V}{V_E} \qquad (19)$$

or

$$\eta = \eta_c + \eta_e + \eta_n \qquad (20)$$

From (19), (20), and (12), with $C_D = 2\sin^2\theta_c$, corresponding to the Newtonian drag coefficient of a cone at zero angle of attack,[3]

$$\eta_e = \int_o^1 C_e V^{q-3}\rho^{p-1}\frac{r_b}{\rho_o}\frac{\tan^2\theta_w - \tan^2\theta_c}{3\tan^3\theta_c\sin^2\theta_c}(\sin\theta_w)^q\frac{V}{V_E}\,d\,\frac{V}{V_E} \qquad (21)$$

Assuming that the cone angle and base radius are constant during entry and that the bow wave angle is independent of speed, we write, noting that $V/V_E = U/U_E$,

$$\eta_e = \frac{r_b}{\rho_o^p}\frac{\tan^2\theta_w - \tan^2\theta_c}{3\tan^3\theta_c\sin^2\theta_c}\left[C_{e_1}V_E^{q_1-3}(\sin\theta_w)^{q_1}\int_o^{\frac{U_{1,2}}{U_E}}\rho^{p-1}\left(\frac{U}{U_E}\right)^{q_1-2}d\left(\frac{U}{U_E}\right)\right.$$
$$\left. + C_{e_2}V_E^{q_2-3}(\sin\theta_w)^{q_2}\int_{\frac{U_{1,2}}{U_E}}^1\rho^{p-1}\left(\frac{U}{U_E}\right)^{q_2-2}d\left(\frac{U}{U_E}\right)\right] \qquad (22)$$

If a constant altitude is maintained during entry, ρ is constant and equation (22) may be integrated to obtain

$$\eta_e = r_b\frac{\rho^{p-1}}{\rho_o^p V_E^2}\frac{(\tan^2\theta_w - \tan^2\theta_c)\sin\theta_w}{3\tan^3\theta_c\sin^2\theta_c}\left\{\frac{C_{e_1}U_{1,2}^{q_1-1}}{q_1-1} + \frac{C_{e_2}U_{1,2}^{q_2-1}}{q_2-1}\left[\left(\frac{U_E}{U_{1,2}}\right)^{q_2-1} - 1\right]\right\} \qquad (23)$$

where

$$\frac{C_{e_1}U_{1,2}^{q_1-1}}{q_1-1} = 2.55\times10^{10} \qquad \frac{J}{m^4} \equiv \frac{kg}{(m\cdot s)^2}$$

and

$$\frac{C_{e_2}U_{1,2}^{q_2-1}}{q_2-1} = 9.02\times10^{10} \qquad \frac{J}{m^4}$$

[3]The question of how such a cone can develop the lift force generally necessary for hyperbolic grazing entry will be discussed in a later section.

Alternatively, if the Reynolds number is maintained constant along the trajectory, ρV is approximately constant and

$$\eta_e = \frac{(\rho V)^{p-1}}{V_E^2} \frac{r_b}{\rho_o}^p \frac{(\tan^2 \theta_w - \tan^2 \theta_c)(\sin \theta_w)^p}{3 \tan^3 \theta_c \sin^2 \theta_c} \left\{ \frac{C_{e_1} U_{1,2}^{q_1-p}}{q_1 - p} + \frac{C_{e_2} U_{1,2}^{q_2-p}}{q_2 - p} \left[\left(\frac{U_E}{U_{1,2}} \right)^{q_2-p} - 1 \right] \right\} \tag{24}$$

where

$$\frac{C_{e_1} U_{1,2}^{q_1-p}}{q_1 - p} = 1.32 \times 10^7 \quad \frac{W}{m^3} \left(\frac{s}{m} \right)^{1.80}$$

and

$$\frac{C_{e_2} U_{1,2}^{q_2-p}}{q_2 - p} = 5.51 \times 10^7 \quad \frac{W}{m^3} \left(\frac{s}{m} \right)^{1.80}$$

In equations (23) and (24), when $U_E < U_{1,2}$, $U_{1,2}$ is to be replaced by U_E.

The nonequilibrium contribution to η is written by use of equations (19), (20), and (15)

$$\eta_n = C_n V_E^{s-3} \left(\frac{\tan \theta_w}{\tan \theta_c} \right)^2 \frac{(\sin \theta_w)^{s-1}}{\sin^2 \theta_c} \int_0^1 \frac{(V/V_E)^{s-2}}{\rho} \left(\frac{\bar{\rho}}{\bar{\rho}_{cl}} \right)^i d \frac{V}{V_E} \tag{25}$$

which, for constant altitude entry, becomes

$$\eta_n = \frac{C_n V_E^{s-3}}{\rho(s-1)} \left(\frac{\tan \theta_w}{\tan \theta_c} \right)^2 \frac{(\sin \theta_w)^{s-1}}{\sin^2 \theta_c} \left(\frac{\bar{\rho}}{\bar{\rho}_{cl}} \right)^i \tag{26}$$

and for constant Reynolds number entry

$$\eta_n = C_n V_E^{s-3} \left(\frac{\tan \theta_w}{\tan \theta_c} \right)^2 \frac{(\sin \theta_w)^{s-1}}{\sin^2 \theta_c} \left\{ \frac{1}{\bar{\rho}_{cl} \rho_o (s-1)} \left[1 - \left(\frac{V_{cl}}{V_E} \right)^{s-1} \right] + \frac{V_E}{(\rho V) s} \left(\frac{V_{cl}}{V_E} \right)^s \right\} \tag{27a}$$

For the cases of interest here, it is generally permissible to simplify equation (27a) to

$$\eta_n = \frac{C_n V_E^{s-2}}{(\rho V) s} \left(\frac{\tan \theta_w}{\tan \theta_c} \right)^2 \frac{(\sin \theta_w)^{s-1}}{\sin^2 \theta_c} \tag{27b}$$

where ρV is a constant of the motion.

The laminar convective portion of η is written by use of equations (16), (18), (19), and (20)

$$\eta_c = \frac{C_c \sqrt{\sin 2\theta_c}}{V_E^2 \sqrt{r_b} \sin^2 \theta_c} \int_0^{V_E} \left(\frac{1 - \sigma}{1 + K_c V^2} + \sigma \right) \frac{V^{j+1} \, dV}{\sqrt{\bar{\rho}}} \tag{28}$$

This integral cannot be evaluated in closed form for arbitrary noninteger values of j. However, it can be readily evaluated numerically. For constant altitude entries, the constant $\sqrt{\bar{\rho}}$ is taken outside the integral; the integral is then a function of V_E and the ablation material constants K_c and σ only.

$$I_c(V_E, K_c, \sigma) = \int_0^{V_E} \left(\frac{1 - \sigma}{1 + K_c V^2} + \sigma \right) V^{j+1} \, dV \tag{29}$$

For given material properties, it need be evaluated one time only, as a function of V_E. Values of this integral normalized on V_E^{j+2} are plotted in figure 1 for the material properties previously tabulated for Teflon and vaporizing quartz and for $\sigma = 0$ and $\sigma = 0.1$. It can be noted that the choice of value for σ is not a critical one for vaporizing quartz within the velocity range considered, but is very important for Teflon at the higher velocities.

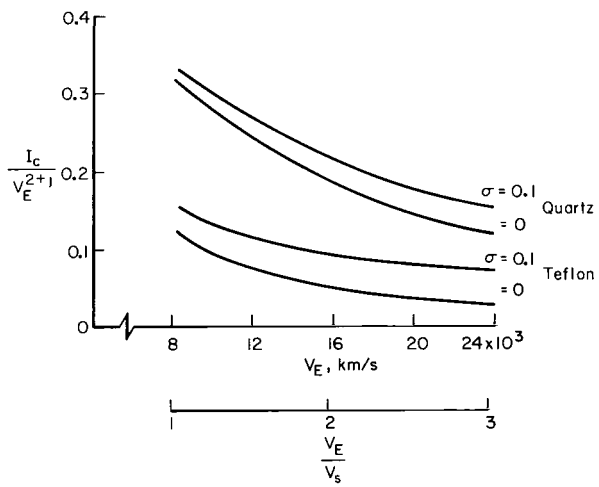

Figure 1.- The laminar convective heating integral for various assumed ablator properties.

On constant Reynolds number trajectories, the integral can be obtained in closed form for the special case $j = 1/6$ by the method shown in appendix B.

Heating Below Satellite Speed

Below satellite speed, only convective heating is important. Since this speed range contributes only a modest fraction of the total heating during the entry, no effort was made to optimize this part of the flight path. (Extensive work dealing with the problem of entry at satellite speed has been reported in the literature.)

For constant Reynolds number trajectories it was assumed that the constant Reynolds number flight path was maintained to terminal velocity. In actuality, as will be shown, such a trajectory can be followed only to the point where $V_y = V$. However, this occurs at very low speed - a few hundred feet per second for the larger bodies, a few thousand feet per second for the smaller ones - and the heat input below this speed is an insignificant part of the total, so no appreciable error results from the assumption.

For the constant altitude trajectories the constant altitude flight paths were followed to somewhat below satellite speed where they were matched in

velocity and altitude to zero-lift ballistic decay trajectories originating at satellite speed above the atmosphere. A small discontinuity in γ that occurs at the matching point was ignored. The time history of the coordinates of this kind of flight path are tabulated in reference 15. The convective heat-transfer relation, equation (28), was applied to the appropriate portion of these trajectories. The maximum acceleration is 8.3 g, making the satellite speed descent trajectory suitable for manned vehicles.

Trajectory Analysis

The choice of trajectories was important to the analysis. The constant altitude deceleration and constant Reynolds number descent trajectories were selected to simplify the heating analysis as well as to permit studies of parametric variations in vehicle size, density, cone angle, etc., on similar flight paths. At the same time they are representative of the heating on shallow angle entry. Trajectory types considered in some earlier work, such as constant lift-drag ratio trajectories, are, by comparison, complicated by altitude excursions (skipping motions), lack generic similarity, and can be analyzed only numerically. One of the types chosen here, the constant Reynolds number descent, is thought to present the minimum heat input to bodies of optimum cone angle. As such, it is a useful standard of comparison.

The objectives of the trajectory analysis were to determine the feasibility of the trajectories for real applications, to supply needed constants for the heating analysis (free-stream density, primarily), and to obtain closed-form expressions for the usual trajectory variables of range, acceleration, velocity, etc., as functions of time. The feasibility of the trajectory is largely determined by the lift-drag ratio required to follow it without exceeding the constraints on acceleration and Reynolds number. The constraints amount to a specification of minimum permissible altitude, in the case of the constant altitude deceleration, and of the altitude at the point of entry onto the constant Reynolds number descent, in the other case.

It was assumed that the lift-drag ratio would be generated by a geometric modification of the cone, such as those described in appendix C. Roll oscillation at the trim attitude provides modulation of the vertical component of L/D, which is required, in general, to be a decreasing function of time.

The principal trajectory equations are given below and developed in appendix D.

Constant altitude deceleration.- The lift-drag ratio required is at every instant a function of the total acceleration and the flight velocity

$$\frac{L}{D} = \frac{\left(\frac{V}{V_s}\right)^2 - 1}{\left[\left(\frac{a}{g}\right)^2 - \left(\frac{V}{V_s}\right)^4\right]^{1/2}} \tag{30}$$

where the total acceleration, the vector sum of that along the path and across the path, is given by

$$\frac{a}{g} = \left(\frac{V}{V_s}\right)^2 \left\{ \left[\frac{\rho V_s^2}{2(W/C_D A)} \right]^2 + 1 \right\}^{1/2} \tag{31}$$

and $W/C_D A$ may be written in terms of the cone angle, mean body density, and base radius.

$$\frac{W}{C_D A} = \frac{\rho_b r_b g}{6 \sin^2 \theta_c \tan \theta_c} \tag{32}$$

When the total acceleration is limited to a specified value, a_l, the corresponding L/D is given by equation (30), and the ambient density at the flight altitude may be obtained from equations (31) and (32) as

$$\rho = \frac{\rho_b r_b g}{3 V_s^2 \sin^2 \theta_c \tan \theta_c} \left[\frac{(a_l/g)^2}{(V_E/V_s)^4} - 1 \right]^{1/2} \tag{33}$$

If a Reynolds number limit rather than the acceleration limit determines the altitude, the density is given by

$$\rho = Re_l \frac{\tan \theta_c}{k} \frac{\mu}{V_E r_b} \tag{34}$$

where

$$k \equiv \frac{Re_\epsilon}{Re} \tan \theta_c \tag{35}$$

is approximately constant and equal to 2 for $U < V_s$ (appendix D). For $U > V_s$, k takes on smaller values, going to about 1.3.

The velocity-distance, velocity-time, and time-distance relations are

$$\frac{V}{V_E} = e^{-\frac{1}{2} \frac{C_D A}{m} \rho x} \tag{36}$$

$$V = \frac{V_E}{1 + \frac{1}{2} \frac{C_D A}{m} \rho V_E t} \tag{37}$$

and

$$e^{\frac{1}{2} \frac{C_D A}{m} \rho x} = 1 + \frac{1}{2} \frac{C_D A}{m} \rho V_E t \tag{38}$$

respectively, where x is arc distance along the orbital path. Fixing the maximum acceleration and the entry velocity can be shown to determine $(C_D A/m)\rho$. Hence, for given maximum acceleration and entry velocity, the x - t and V - t relations are universal.

Constant Reynolds number descent.- Appendix D shows that to maintain a constant Reynolds number requires a constant rate of descent, V_y = constant, given by

$$V_y = \frac{C_D A}{m} \frac{(\rho V)}{2\beta} \tag{39}$$

where ρV is a constant and β is the reciprocal of the atmospheric scale height. The angle of descent is not constant, however, being defined by

$$\sin \gamma = \frac{V_y}{V} \tag{40}$$

where V decreases with increasing time.[4] The angle of descent increases until, in some cases, $V_y = V$ and $\gamma = 90^\circ$. At this point, the motion is governed by the equations of simple ballistic descent and it is no longer possible to maintain the Reynolds number constant.

The lift-drag ratio is governed by equation (D34), which may be simplified, for the cases of most practical interest, by use of small angle approximations for the sine and cosine of the flight-path angle to obtain

$$\frac{L}{D} = \frac{1 - (V_s/V)^2}{\beta R_p (V_y/V)} + \frac{V_y}{V} \tag{41}$$

where R_p is the radius of the earth or other planet whose atmosphere is entered. The total acceleration may be written

$$\frac{a}{g} = \left(\frac{V}{V_s}\right)^2 \left\{ \left[\frac{(\rho V) V_s}{2(V/V_s)(W/C_D A)} \right]^2 + \left[\beta R_p \left(\frac{V_y}{V}\right)^2 + 1 \right]^2 \right\}^{1/2} \tag{42a}$$

which may also be put in terms of the rate of descent to obtain

$$\frac{a}{g} = \left[\left(\frac{V_y}{V_s}\right)^4 (\beta R_p)^2 + \left(\frac{V}{V_s}\frac{V_y}{V_s}\right)^2 [(\beta R_p)^2 + 2\beta R_p] + \left(\frac{V}{V_s}\right)^4 \right]^{1/2} \tag{42b}$$

Finally, the relations between velocity and time, velocity and distance, and time and distance are, respectively,

---

[4]The heating occurs predominantly at velocities greater than $V_E/4$ and, in this range, sin γ is smaller than 4 sin γ_E (eq. (40)). The magnitude of γ_E is defined by equations (39) and (40), and it is found that V_y/V_E is, for cases of interest, a very small number, corresponding to angles smaller than a degree. Hence, the use of small flight-path angle approximations for L/D is justified, and the neglect of the weight force component in equation (4) is also valid.

$$\frac{V}{V_E} = e^{-\frac{C_D A}{m}\frac{(\rho V)}{2}t} \tag{43}$$

$$V = V_E - \frac{C_D A}{m}\frac{(\rho V)}{2}x \tag{44}$$

$$x = \frac{2V_E}{(\rho V)}\frac{m}{C_D A}\left(1 - e^{-\frac{C_D A}{m}\frac{(\rho V)}{2}t}\right) \tag{45}$$

where, again, ρV in equations (43) to (45) is a constant.

PRESENTATION OF RESULTS

Trajectories

Constant altitude.- Ambient densities and flight altitudes dictated by the acceleration and Reynolds number limits are shown in figure 2 as a function of entry velocity for representative values of the governing parameters. The steeper family of curves is the acceleration-limited set. The intersections of this family with the Reynolds number limited family define points of transition from Reynolds number to acceleration governed altitudes. Consider the two dashed curves, for example. At entry velocities below $1.66\,V_s$, the Reynolds number requires the lower density and governs, while above this velocity, the acceleration limit governs. For a 30° cone with a base radius of 3.05 m, the Reynolds number limits corresponding to the three curves are 10^7, 5×10^6, and 10^6, respectively. For the same radius and cone angle, the acceleration curves represent body densities of 640, 320, and 160 kg/m^3, top to bottom. For these conditions, then, a Reynolds number limit of 10^6 would govern altitude selection for the entire range of entry velocities considered.

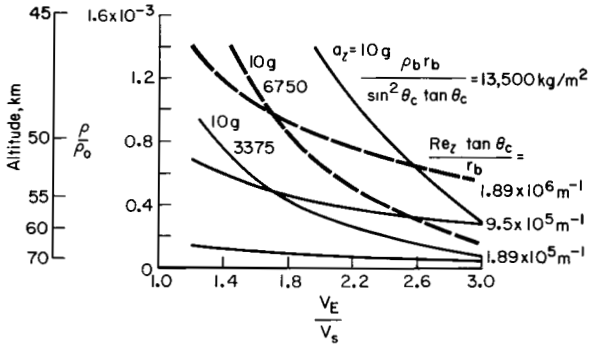

Figure 2.- Ambient densities and altitudes dictated by acceleration and Reynolds number limits.

Entry may take place at higher altitudes than those calculated, but not at lower altitudes without violating the imposed limits on acceleration and Reynolds number. The altitudes shown, therefore, represent undershoot limits. The overshoot limits, not shown, depend on the available L/D. The undershoot boundary, however, is the altitude of interest for this analysis, since it minimizes the total heat input for optimum bodies.[5]

[5]Guidance limitations make it necessary that real vehicles be able to withstand entry over a finite corridor. They must therefore be designed to accept somewhat larger heat inputs than the minimum considered here.

The lift-drag ratios needed for maintaining constant altitude flight are shown in figure 3 as a function of velocity for several levels of total acceleration. In general, the maximum L/D is required at the highest velocity,

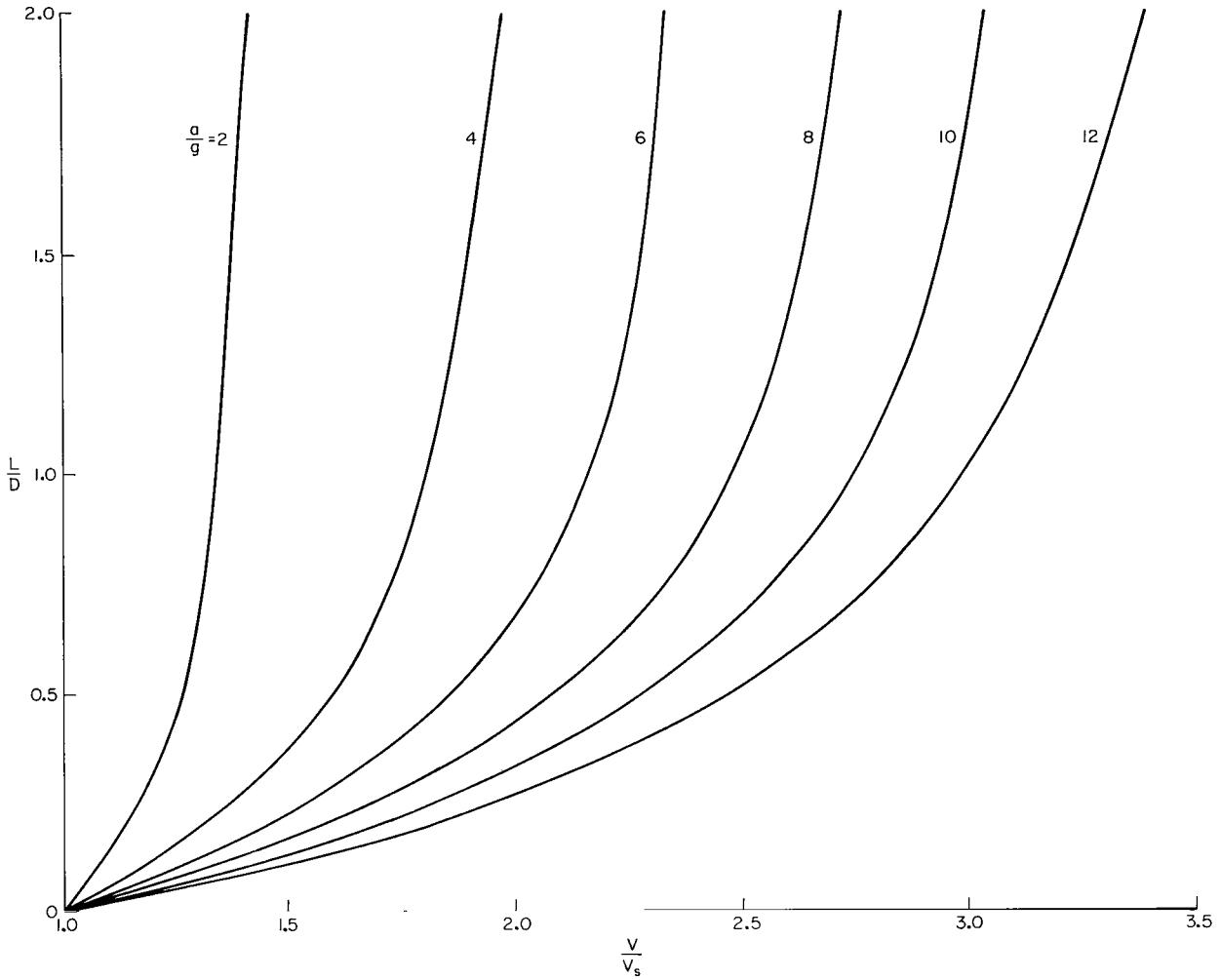

Figure 3.- Lift-drag ratios required on constant altitude trajectories.

that is, at entry in our analysis. A lift-drag ratio of 1 is sufficient to permit a 10 g limit constant altitude entry at a velocity of 2.76 V_s. At higher entry velocities, the L/D required rises rapidly, or, alternatively, the acceleration limit must be increased. For any acceleration level, the L/D curve is asymptotic to a vertical line at a velocity $V_E/V_S = \sqrt{a/g}$. This is the velocity for which the centripetal acceleration is the total acceleration. The entry body is then flying above the atmosphere, but still requires lift to hold it in a circular path; hence, L/D must be infinite.

When the altitude is governed by a Reynolds number limit, or is higher than the minimum altitude permitted, the acceleration is smaller than the acceleration limit. Figure 3 is then entered at the appropriate level of acceleration to define L/D. A consequence of such a situation is that high lift-drag ratios may be required at the lower entry velocities.

The variations of velocity, range, lift-drag ratio, and acceleration with time after entry are shown in figure 4 for an entry velocity of 2.5 V_s and an

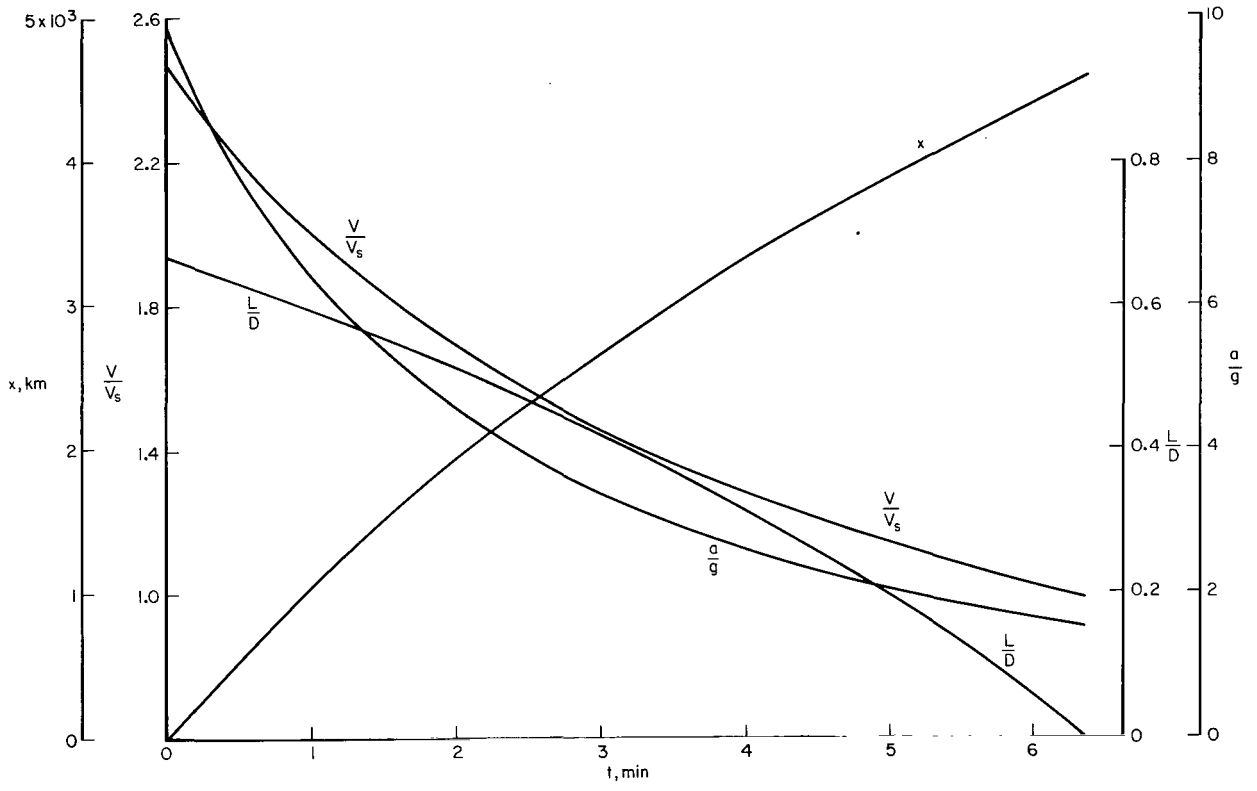

Figure 4.- Representative characteristics of an acceleration-limited constant altitude trajectory, $\alpha_l/g = 10$, $V_E/V_s = 2.5$.

acceleration limit of 10 g, attained at entry. The curves are terminated at satellite velocity. The range covered to this point is 4600 km, and the elapsed time is roughly 6 minutes. The lift-drag ratio and total acceleration decrease continuously with time, the former going to zero at satellite velocity.

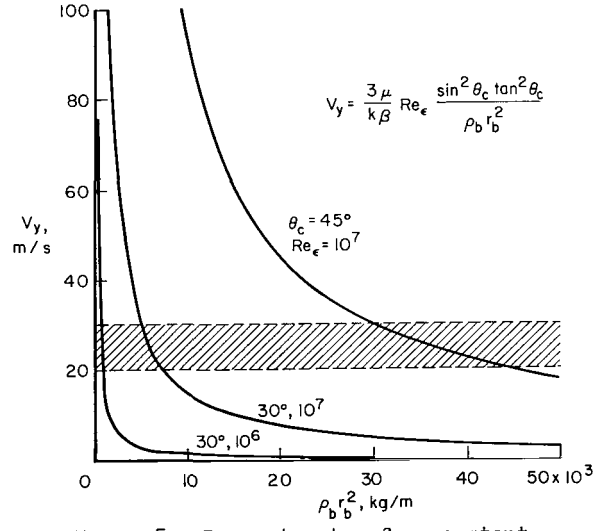

Figure 5.- Descent rates for constant Reynolds number as a function of body density and size.

The curves in figures 2 and 4 are examples. Other cases of interest may be readily obtained from the trajectory equations.

Constant Reynolds number.- The descent rates characteristic of constant Reynolds number trajectories are plotted in figure 5 as a function of the body density times the base radius squared, for two cone angles and two values of the Reynolds number. The equation given in the figure is an

alternate form of equation (39) which incorporates equations (32) and (35). Large or dense bodies tend to have quite low rates of descent to maintain constant Reynolds number. The assumptions cited earlier concerning small angles of descent are amply satisfied by the conditions in this figure.

The lift-drag ratios required are plotted in figure 6 as a function of flight velocity for various rates of descent. At V_y less than about 25 m/s, the required lift-drag ratio starts to become large, and may exceed that which is available. The accelerations, on the other hand, are minimized by use of small descent rates (fig. 7) and 25 m/s is, fortuitously, again near the boundary for acceptable levels of acceleration at the higher entry velocities. Thus, to satisfy the requirements on both L/D and acceleration, values of V_y must lie in the vicinity of 25 m/s. A band in figure 5 indicates this acceptable region. Values of body density and base radius to which it corresponds depend on the cone angle and Reynolds number chosen and may be calculated from the equation in this figure.

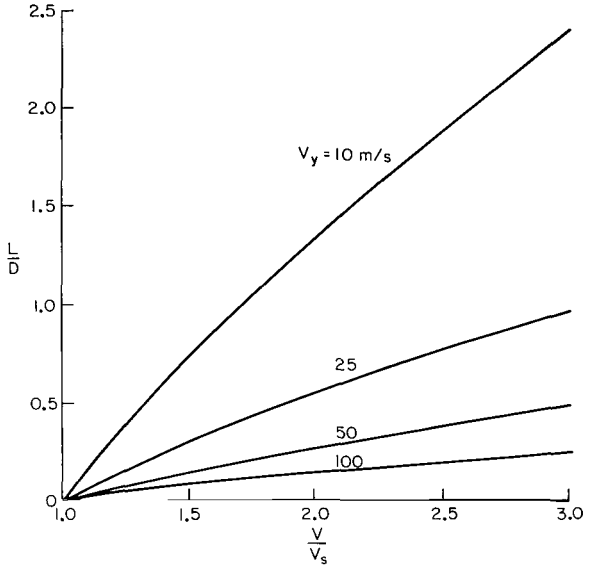

Figure 6.- Lift-drag ratios required on constant Reynolds number descents.

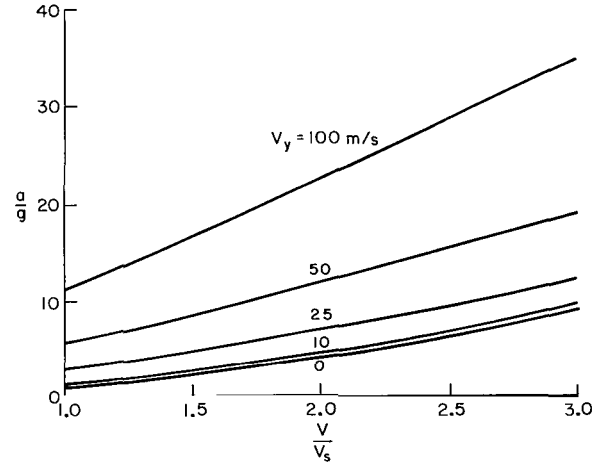

Figure 7.- Acceleration on constant Reynolds number descents.

An example of a constant Reynolds number descent that satisfied reasonable requirements on acceleration and L/D is shown in figure 8. The body size and density give a value of the parameter $\rho_b r_b^2$ of 2980 kg/m. For a cone angle of 30° and a Reynolds number of 5 million, the descent rate, according to figure 5, is 27 m/s. The trajectory variables in figure 8 show a descent to satellite velocity in 4 minutes from an entry velocity of 2.5 V_s with a maximum acceleration of 9.8 g, a maximum L/D of 0.7, and a flight range of 3150 km. The angle of descent is 0.08° initially, increasing to 0.2° at satellite velocity. Following a trajectory with such precision may, in practice, present a problem in flight-path control. In principle, however, such trajectories appear feasible.

Heating

Constant altitude entries.- The total heat input energy fraction to cones of large base radius with 30° and 35° half-angles is shown in figures 9 as a function of entry velocity. For the conditions cited, the total heat input

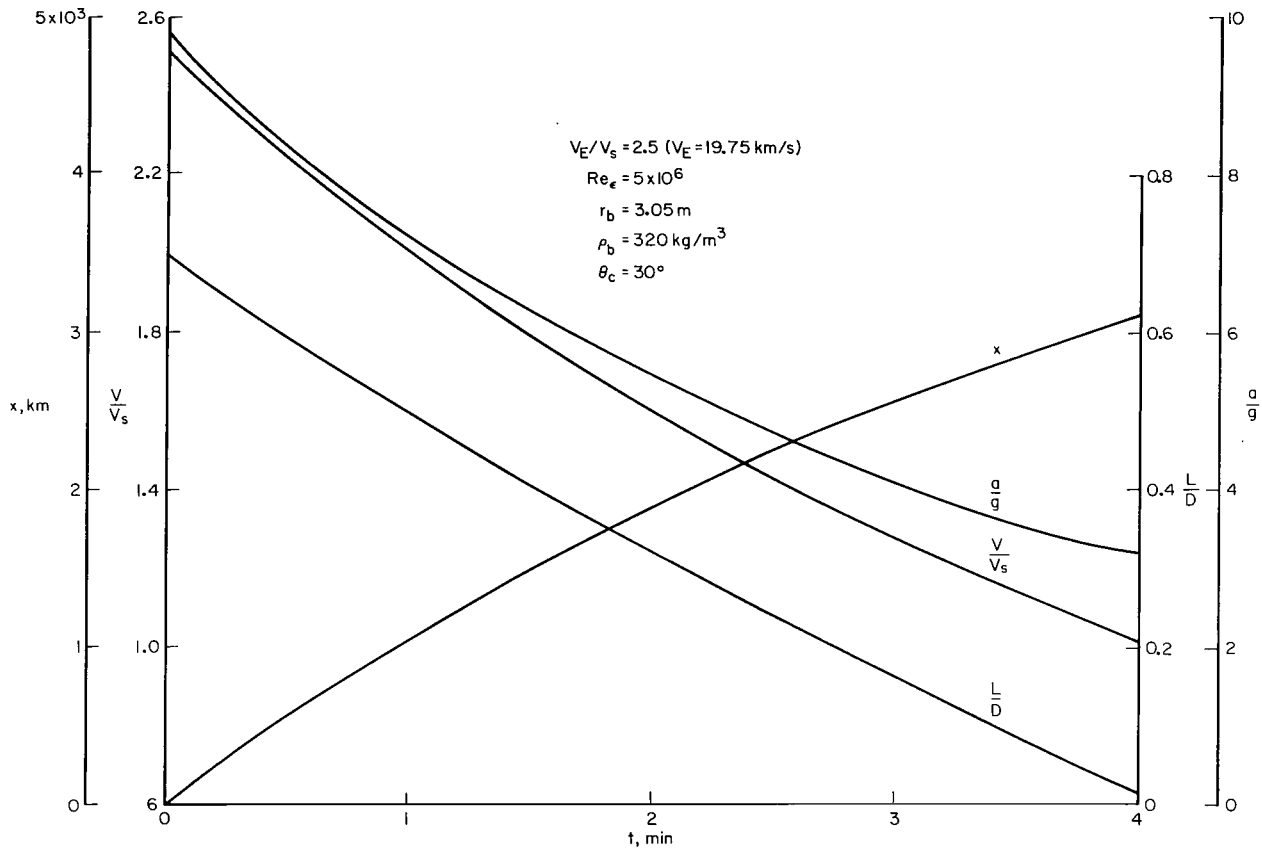

Figure 8.- History of a constant Reynolds number descent.

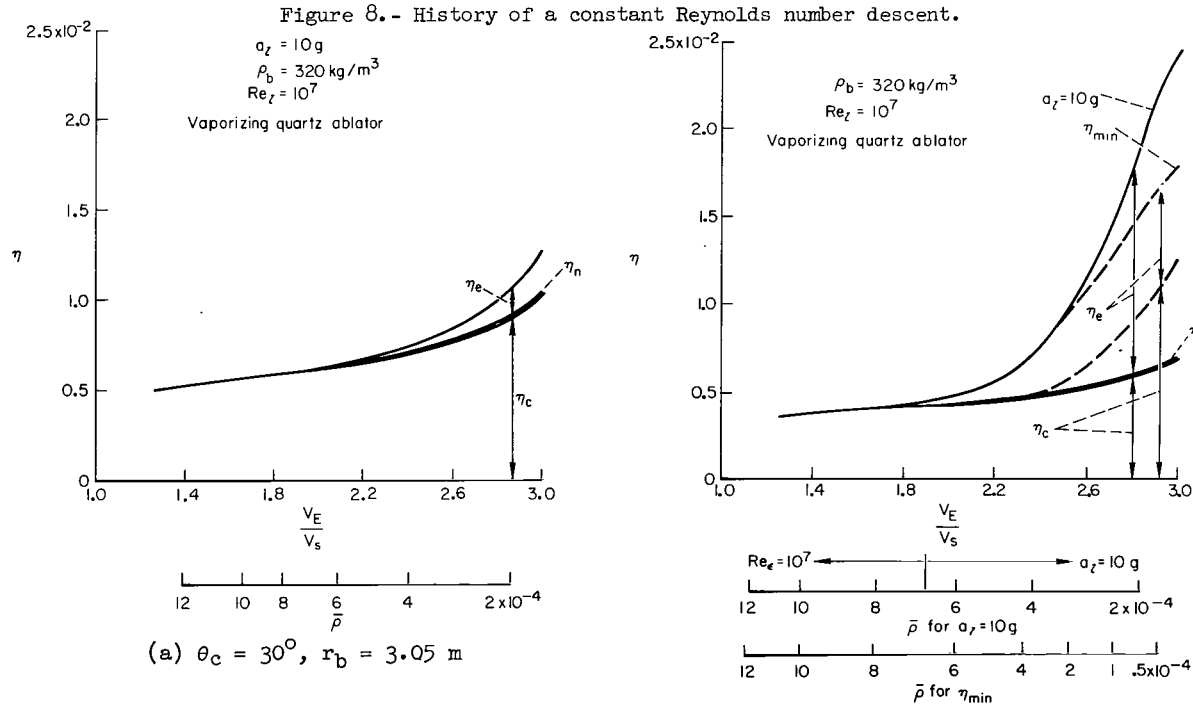

(a) $\theta_c = 30°$, $r_b = 3.05$ m

(b) $\theta_c = 35°$, $r_b = 4.57$ m

Figure 9.- Variation of the heat input energy fractions with entry velocity on constant altitude entry.

ranges from 0.4 to 2.5 percent of kinetic energy at entry, increasing with increasing V_E, and depending also on the cone angle and base radius.

Laminar convective heating predominates in the case of the 30° cone with a base radius of 3.05 m (fig. 9(a)). The equilibrium radiative heating is kept small by the obliquity of the shock wave. The nonequilibrium radiative contribution is essentially negligible.

For the 35° cone with a base radius of 4.57 m (fig. 9(b)), however, equilibrium radiative heating becomes important at the higher entry velocities and, at $V_E = 3\ V_s$, contributes more heat input than the convection. Note that two sets of curves are shown for the 35° cone. One (the solid lines) corresponds to entries at the 10 g acceleration limited boundary, and the other (dashed lines) to entries at higher altitudes. When the radiative heating is large, minimum total heating occurs at an altitude higher than that for the given acceleration and Reynolds number limits. This minimum is shown by the dashed curve labeled η_{min}. The ambient air densities at the flight altitudes are given in auxiliary scales along the abscissa.

The total heating energy fractions for cone angles from 20° to 60° are given in figure 10, with the base radius, body density, and heat-shield properties fixed. The minimum envelope of these curves gives the minimum value of heat input energy fraction that can be attained at each entry velocity for the conditions specified. The large angled cones depart from this minimum with increasing entry velocity and, as a result of their large radiative heat inputs, attain values of η much larger than the minimum. The optimum cones have half-angles slightly less than 25° at $V_E = 3\ V_s$ and near 30° over a substantial part of the entry velocity range considered.

Presenting the energy fraction as a function of cone angle, as in figure 11, is useful for defining more precisely the optimum cone angle and the minimum energy fraction. In the case shown, which is typical of large limit Reynolds numbers, the minimum heat input within the given limits occurs at the intersection of Reynolds number-limited and acceleration-limited curves. Thus, the optimum cases attain the limiting values of both the acceleration and the Reynolds number at entry. On the dashed portions of the curves, one or the other of the limits is exceeded. Therefore, the minimum point in the $Re_\ell = 10^7$ curve, for example, cannot be utilized.

The definition of the optimum at higher and lower values of the limit Reynolds number is illustrated in figure 12. Curves are shown of η as a function of θ_c for four sets of altitudes corresponding to limit Reynolds numbers from 10^5 to 10^8. At small cone angles, where radiative heating is negligible, η varies on these curves inversely with $(\tan \theta_c)^{3/2}$ according to equations (28) and (34). At larger cone angles, η increases as the radiative heat input becomes important. Hence, each curve for a given Reynolds number limit exhibits a minimum. A fifth curve shows η as a function of θ_c with altitude determined by the acceleration limit. In this case, η is independent of θ_c at small cone angles, where radiation is negligible (eqs. (28) and (33)), rising as cone angle is increased to the region of important radiative heating.

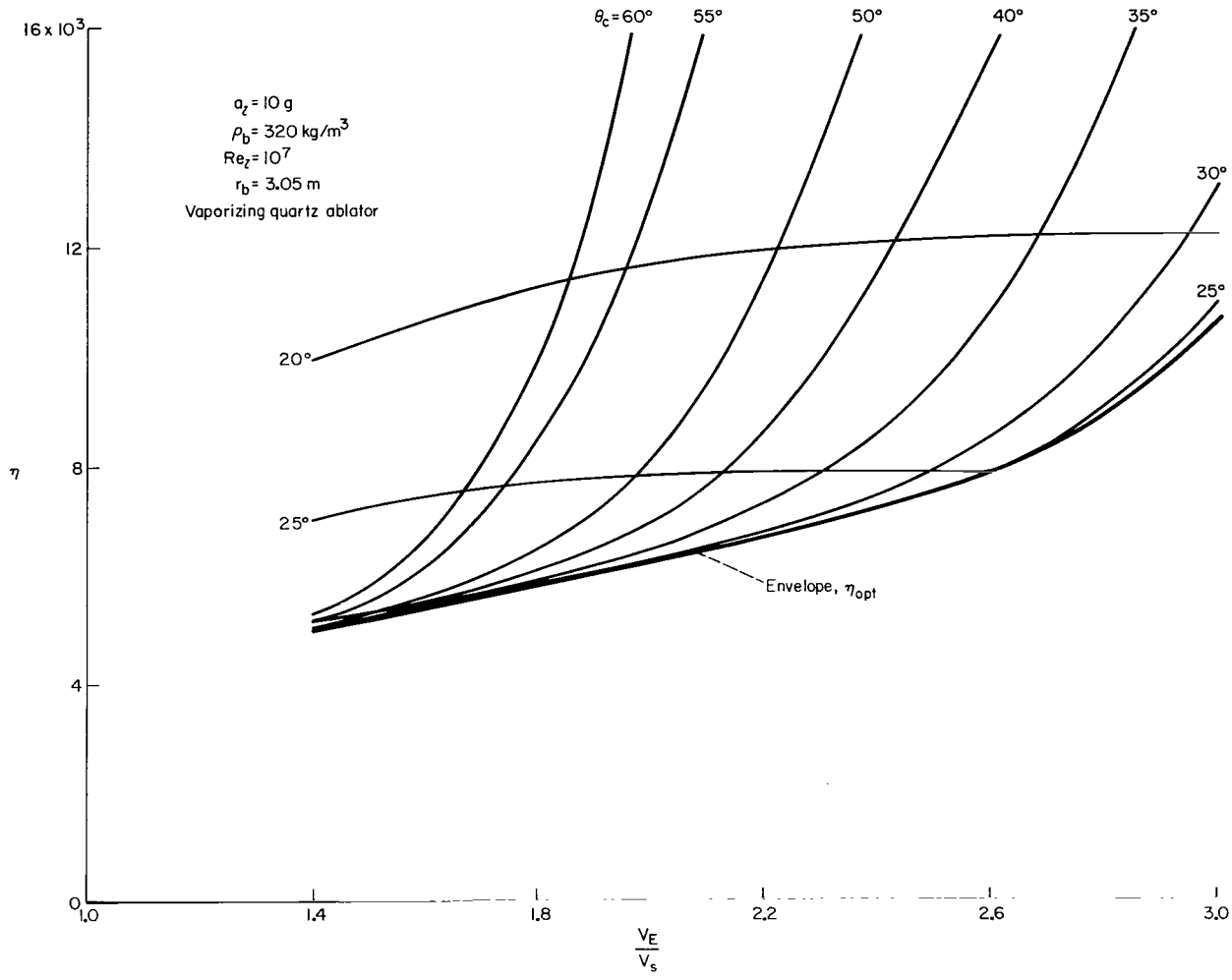

Figure 10.- Variation of heat input energy fraction with entry velocity for cones of various angles on constant altitude trajectory.

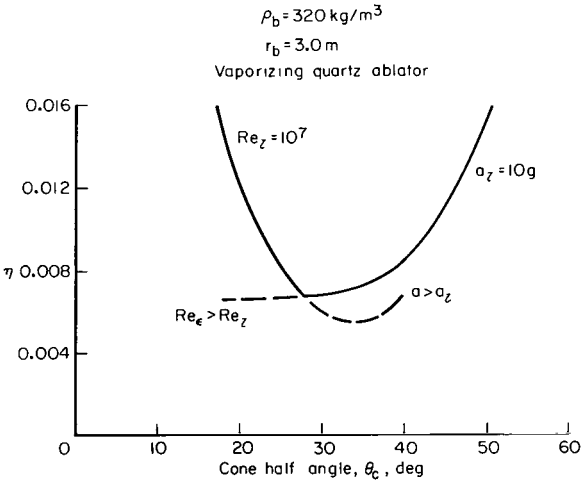

Figure 11.- Variation of heating with cone angle on constant altitude trajectory, V_E/V_s = 2.2.

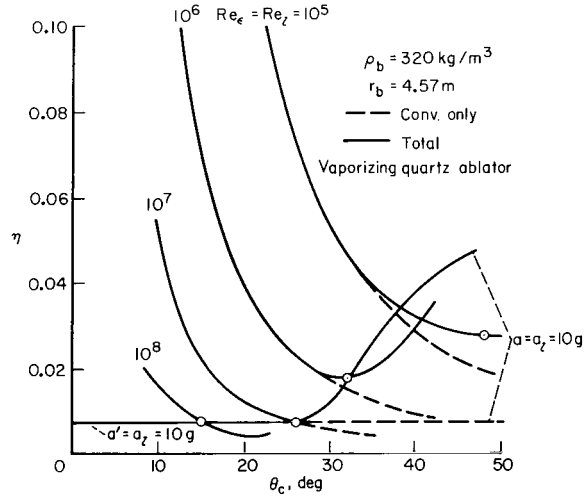

Figure 12.- Effect of limit Reynolds number on optimum energy fraction and cone angle for V_E = 3 V_s.

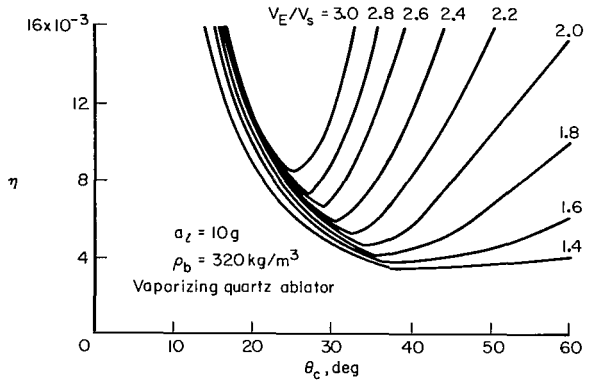

(a) r_b = 4.57 m

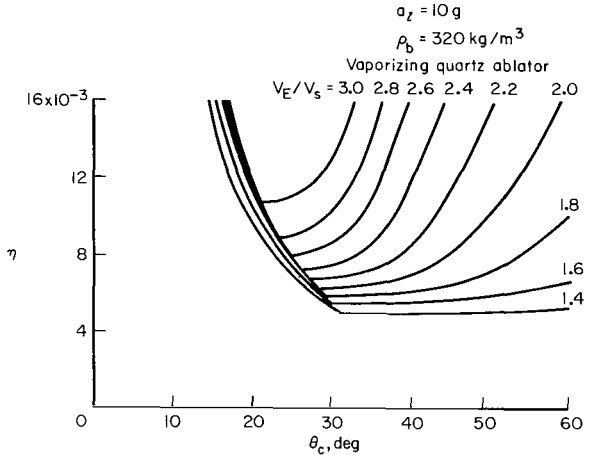

(b) r_b = 3.05 m

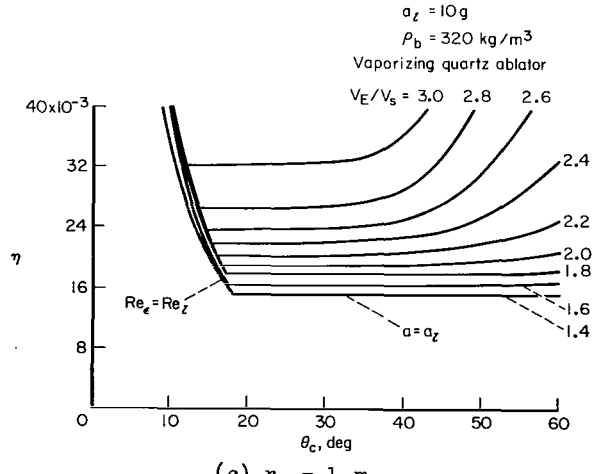

(c) r_b = 1 m

Figure 13.- Definition of minimum heat input and optimum cone angle for bodies of three base radii at $Re_\ell = 10^7$.

The values of minimum η within the simultaneous limitations on acceleration and Reynolds number are shown by the circled points for the four values of Re_ℓ. At $Re_\ell = 10^8$ and 10^7, the optimum occurs in the region of small radiative heating, and is similar to that discussed in figure 11. At $Re_\ell = 10^6$ and 10^5, the optimum has a significant radiative contribution, and occurs on the Reynolds number limited curve at an altitude above that for the acceleration limit. For example, at $Re_\ell = 10^5$, the optimum occurs at a flight altitude greater than that for a_ℓ = 10 g. This is shown by the values of η_c, the dashed curves. (Note that $\eta_c \sim 1/\sqrt{\bar{\rho}}$, eq. (28).) The peak acceleration at the optimum point for this Reynolds number limit is, in fact, only about 1.5 g. Hence, it is seen that the optimum point need not occur at accelerations as large as the acceleration limit. However, the Reynolds number attains its limiting value in every case. Furthermore, lowering the limit Reynolds number below 10^7 can significantly increase the heat input and optimum cone angle, and also, by the arguments of an earlier section, the lift-drag ratio required at entry. The increase in η, however, is not as large as that which would occur with transition to turbulence in the absence of a Reynolds number limit.

Curves like those in figure 11 are given in figures 13 for bodies of three base radii at entry velocities from 1.4 to 3.0 V_s, for a limit Reynolds number of 10^7. These curves define the variation of the minimum energy fraction, which increases with entry velocity, and the optimum cone angle, which decreases with increasing entry velocity. Comparison of figures 13(a), (b), and (c) shows the base radius to be an important variable, and in figure 14, optimum energy fraction is given as a function of base radius for fixed Reynolds number and acceleration limits and body density.

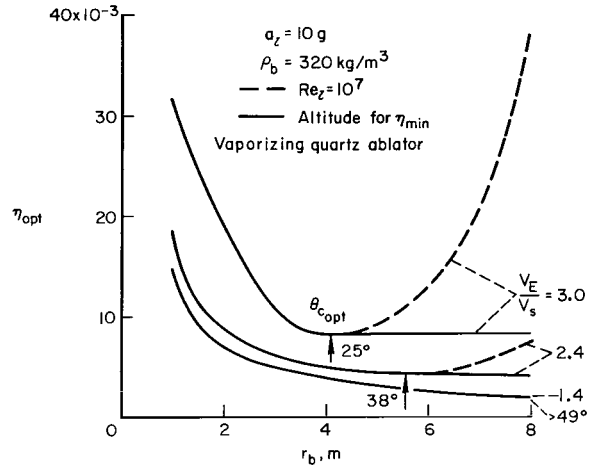

Figure 14.- Dependence of optimum energy fraction on base radius for constant altitude deceleration.

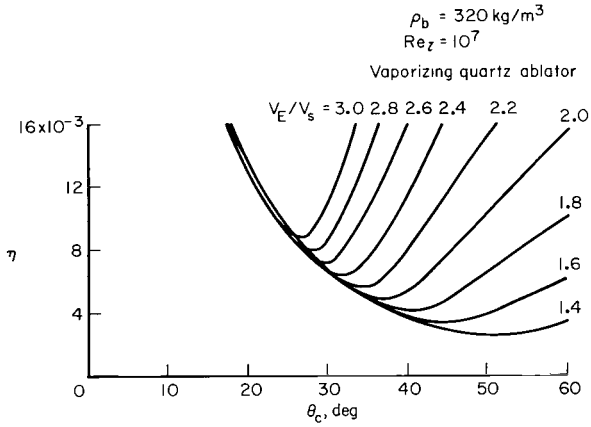

Figure 15.- Energy fractions of a 1-meter base radius body without an acceleration limit.

For small bodies, the optimum cone angle is small, the radiative heating is negligible, and the optimum energy fraction varies inversely with base radius. For large bodies, the optimum cone angle is increased, the radiative heating becomes large, and the optimum energy fraction increases with body size (dashed curves). An optimum base radius is defined. If, in place of the above constraints, the altitude is permitted to go above that dictated by the Reynolds number and acceleration limits to the altitude for minimum total heat input, the solid curves are obtained. On these, the heat input is essentially independent of base radius at large base radii.

The high values of η for the bodies of small base radius are a result of the acceleration limit imposed. Without this limit, the curves on the left of figure 13(c) may be continued to their minimum points to obtain the low values of energy fraction shown in figure 15 with a 1 m base radius. These values would be available to unmanned probes. Note that the Reynolds number limit of 10^7 is still applied.

The body density also enters as a consideration. On acceleration-limited entries, $\eta_c \sim 1/\sqrt{\rho_b}$. Thus, the acceleration-limited curves of figure 13(c) would be lowered a factor of 3 in the small cone angle range by a ninefold increase in body density. There is, therefore, an advantage in the use of dense vehicles in the small size range. With larger bodies (e.g., fig. 11), lowering the acceleration-limited curve allows the Reynolds number-limited curve to govern. The Reynolds number-limited cases are independent of body density. Hence, a small and limited reduction in η is available from body density increases at the larger base radii.

The effect of the limit Reynolds number on optimum energy fraction is shown in figures 16 for large base radius entry bodies at several entry velocities. The second ablation material of the analysis, Teflon, is introduced here for comparison. The characteristic effects of the Reynolds number limit, developed in connection with figure 12, are shown here explicitly. When the Reynolds number limit is high η_{opt} is relatively independent of Re_ℓ, but when the limit is small and the body base radius is large, η_{opt} is sensitive to Re_ℓ and increases as Re_ℓ decreases. The energy fractions remain below

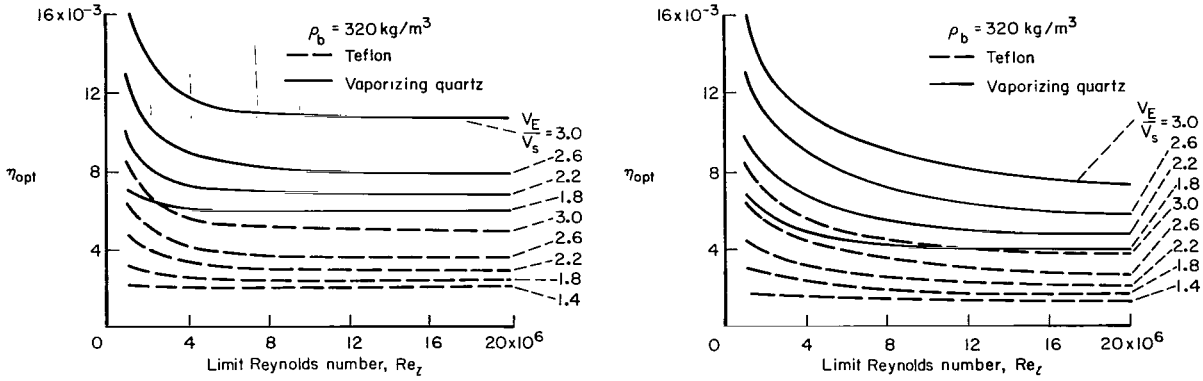

Figure 16.- Variation of optimum energy fraction with limit Reynolds number on constant altitude entries.

0.017, however, for all cases shown, at Reynolds number limits as small as 10^6 and entry velocities to 3 V_s. Optimum cone angles for the conditions of figures 16 are shown in figures 17. The optimum cone angle decreases with increasing entry velocity and with increasing Reynolds number limit, and is relatively insensitive to ablation material.

The low values of energy fraction calculated for Teflon (fig. 16) make that material appear attractive. These values are due, however, to the high blowing rates, that is, high mass loss rates, associated with the low heat of ablation of Teflon. Mass loss curves (figs. 18), in fact, show the order of merit of the two materials and heavily favor the material with large heat of ablation. They also show the effect of changing the limit Reynolds number on the mass loss. The effect of the limit Reynolds number can perhaps be

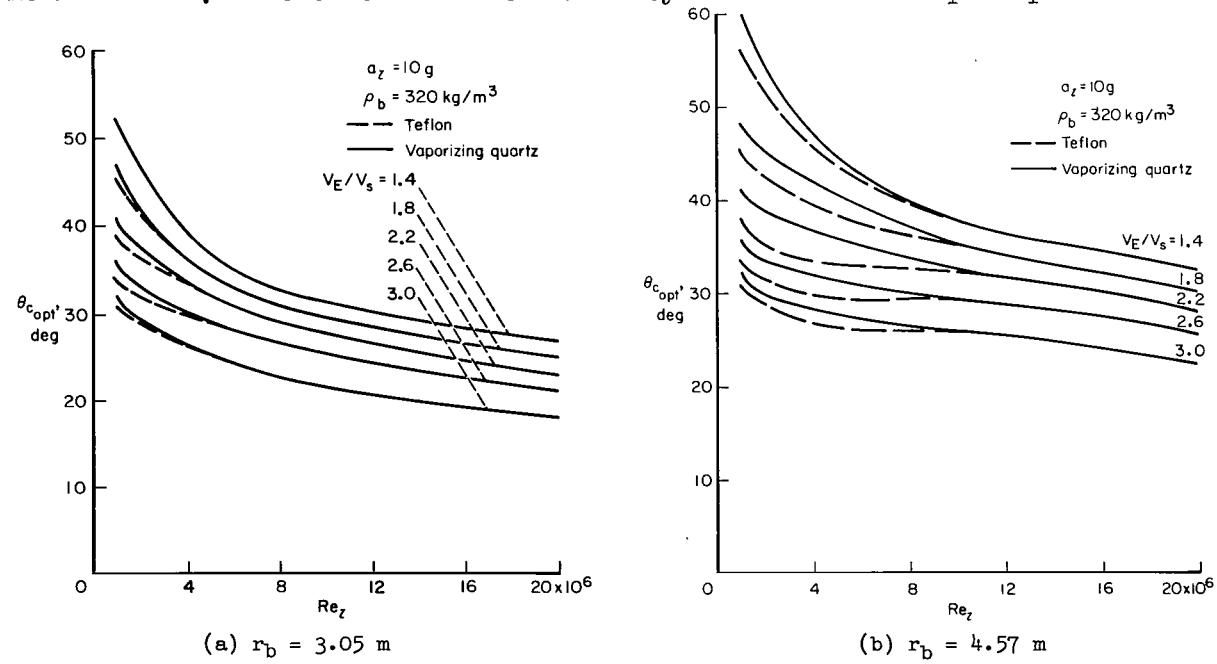

Figure 17.- Optimum cone angle variation with limit Reynolds number and entry velocity for constant altitude entry.

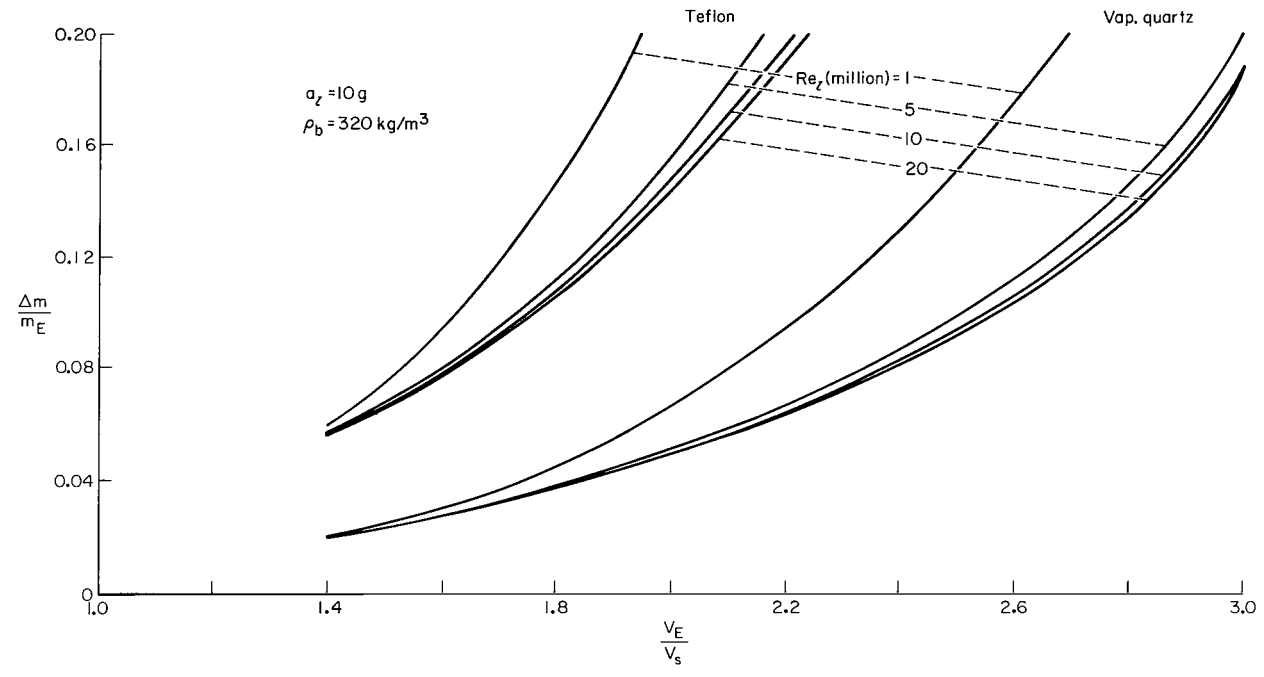

(a) r_b = 3.05 m

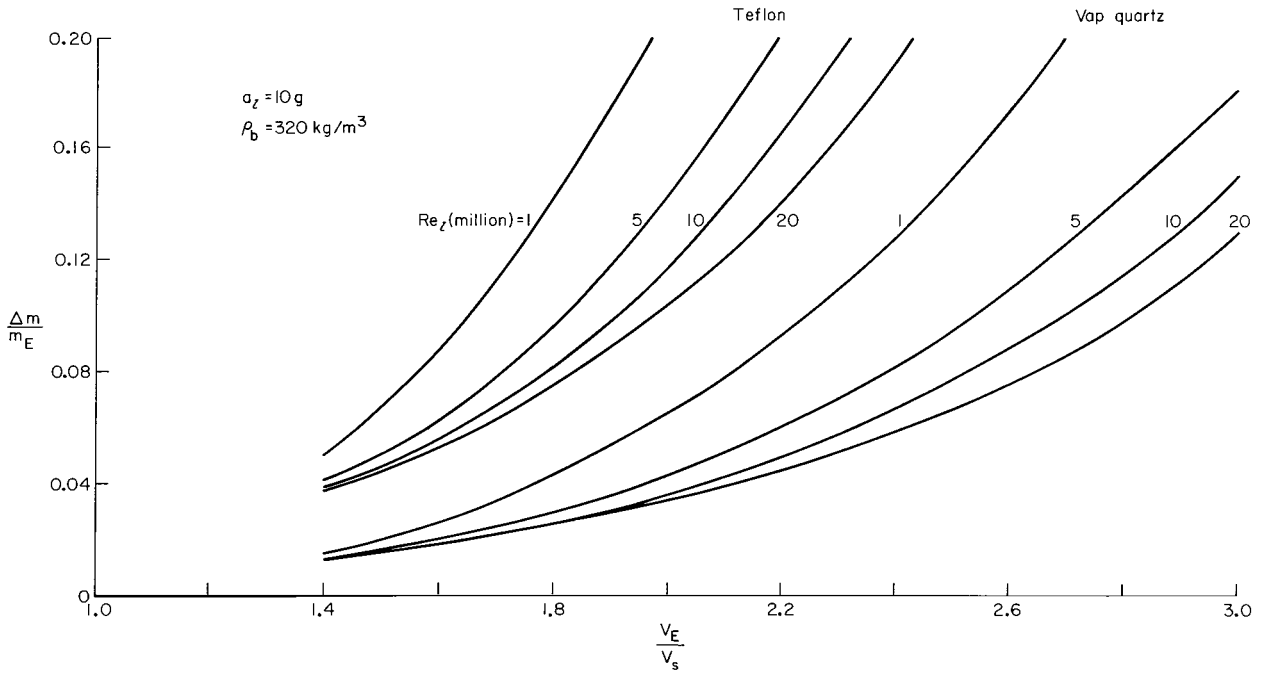

(b) r_b = 4.57 m

Figure 18.- Mass loss ratio on constant altitude entry for two ablation materials.

classified as moderate from 5×10^6 to 20×10^6. Below about 5×10^6 it becomes sizable. Mass losses as small as 20 percent of the entry mass are calculated for entry to three times satellite velocity with vaporizing quartz at $Re_z = 5\times10^6$.

It is noted that if the asymptotic blockage factor σ were taken to be 0 instead of 0.1, the mass losses with Teflon at the higher entry velocities would be approximately halved, while those of quartz would be less affected (fig. 1). Hence, the determination of the correct value of this constant is important.

The other effect of low values of the limit Reynolds number referred to earlier is to increase the lift-drag ratio required. If the lift-drag ratio required exceeds that available, the entry becomes unattainable. The undershoot altitude may then be said to have gone above the overshoot, so that the available entry corridor is negative. Conditions for which this may occur are shown in figures 19, where L/D required at entry is plotted as a function of

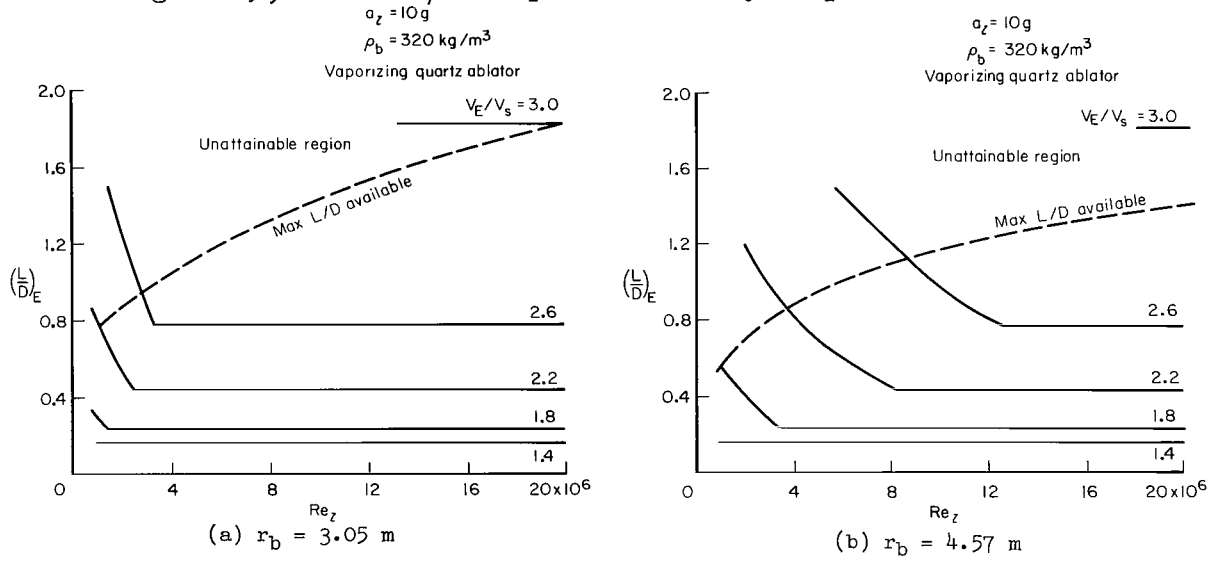

Figure 19.- Limitation on entry velocity imposed by joint consideration of Re_ζ and L/D available.

Reynolds number limit for bodies of two (large) base radii. As long as the acceleration limit is attained at entry, the L/D is, according to equation (30), independent of Reynolds number. This condition is represented by the horizontal sections of the curves. When the acceleration goes below the limiting value, the L/D needed rises rapidly, as on the curve sections at the left. The optimum cone angle also varies with Re_ζ, as in figure 12, and along with it, the available L/D (appendix C). If the L/D required crosses the boundary marked maximum L/D available, it enters the unattainable region. This is seen to be important at the highest entry velocities considered, consistent with figure 3, which shows that L/D becomes marginal at such entry velocities.

Experimental observations of transition in very high enthalpy flow over ablating cones will be needed to determine a suitable value of the parameter Re_ζ.

Constant Reynolds number entries.- While the trajectory analysis showed that constant Reynolds number descents could be made with a 10 g acceleration limit, by designing to a descent rate of 25 m/s, the heating calculations were

not limited to such cases. Interest in the constant Reynolds number trajectory as a minimum heat input trajectory suggested its more general investigation.

Curves similar in form to those presented for constant altitude entry were obtained. Thus, figure 20 shows the effect of entry velocity on the heat input energy fraction for a given local Reynolds number (10^7), cone angle, base radius, and ablation material. (Note that the energy fraction is independent of body density for the constant Reynolds number trajectories.) As with the constant altitude entries, where the radiative contribution is large, Reynolds numbers smaller than the specified value can lower the total heat input.

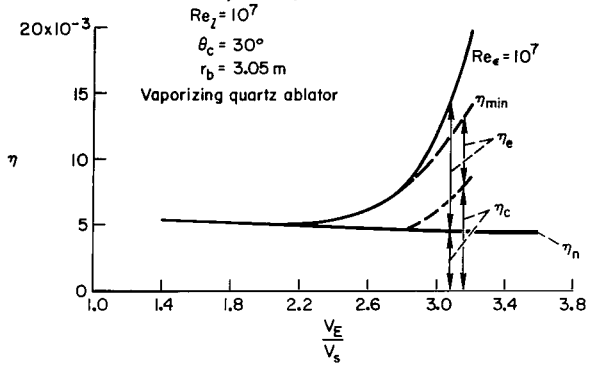

Figure 20.- Typical variation of the heat input energy fractions with entry velocity on constant Reynolds number trajectory.

An interesting feature of figure 20 is that the laminar convective energy fraction, η_c, diminishes with increasing entry velocity. This will occur when σ is small and $K_c V^2$ is large compared to 1. In the limit of $\sigma = 0$, the integral in equation (28) then becomes, for ρV = constant,

$$(\rho V)^{-1/2} \int_0^{V_E} \frac{V^{j+3/2} dV}{K_c V^2} = \frac{V_E^{j+1/2}}{(j + 1/2) K_c \sqrt{\rho V}}$$

and

$$\eta_c \sim 1/V_E^{3/2-j}$$

Figure 21 shows the minimum heat input energy fractions as a function of entry velocity for a series of cone angles at a given Reynolds number, and the envelope of minimum η for these conditions is defined. Figure 22 shows the effect of body base radius and ablation shield properties on the envelope values. The ablation property effect is comparable to that on constant altitude entry, but the base radius effect is small. The convective heating contribution is, in fact, independent of r_b, as may be seen from equation (28) where $(\rho V r_b)^{1/2}$ may be taken outside the integral as a constant (see also eq. (B5)). Furthermore, the radiative contribution is only weakly dependent on r_b, varying as $r_b^{0.2}$ according to equation (24) with $\rho = 1.8$. Hence, unlike the constant altitude entry, the constant Reynolds number entry shows heating energy fractions essentially independent of body size.

The effect of the Reynolds number on the optimum energy fractions is shown in figure 23. The variation in the convective heat input with $Re^{-1/2}$ is the principal part of this dependence, but changes with Reynolds number in the optimum cone angle and radiative input also contribute. The optimum cone angles are shown for four Reynolds numbers and two ablation materials in figures 24. There is some sensitivity to Reynolds number, while the effects of ablation material and body size are minor. In figure 25, mass loss fractions

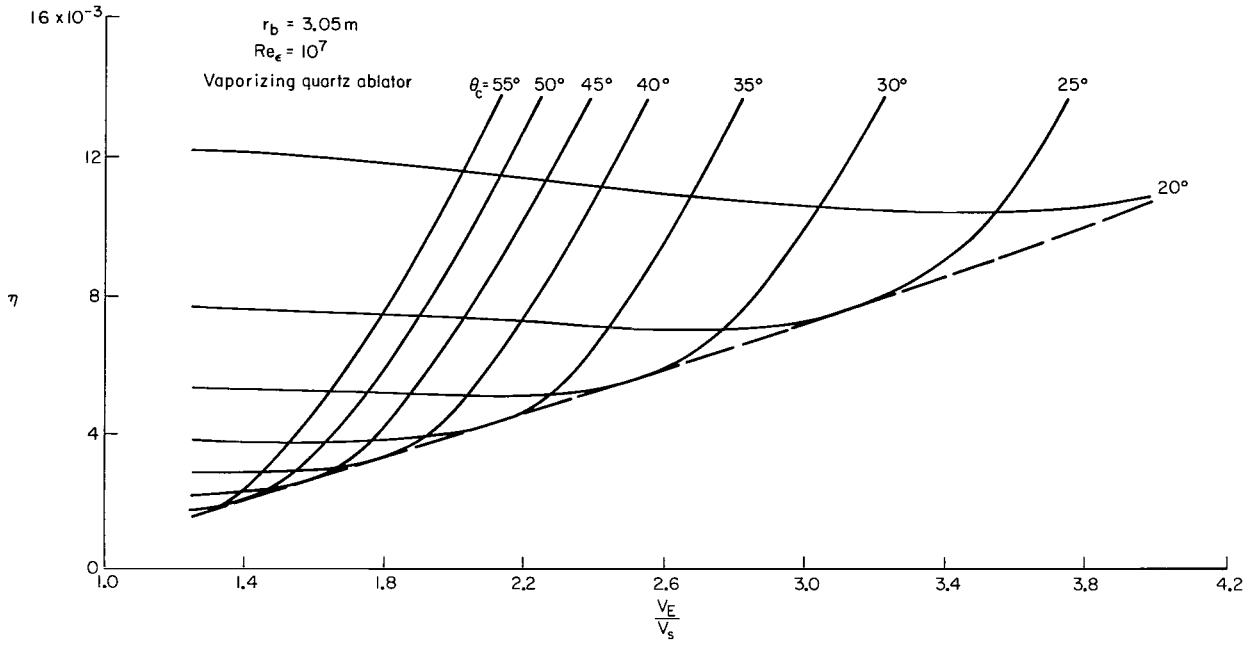

Figure 21.- Variation of the heat input energy fraction with entry velocity for cones of various angles on constant Reynolds number trajectories.

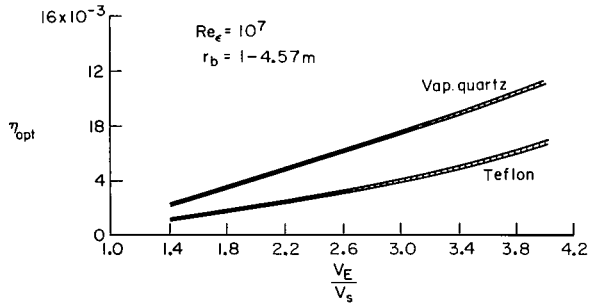

Figure 22.- Effect of base radius and ablation material on optimum energy fraction for constant Reynolds number trajectories.

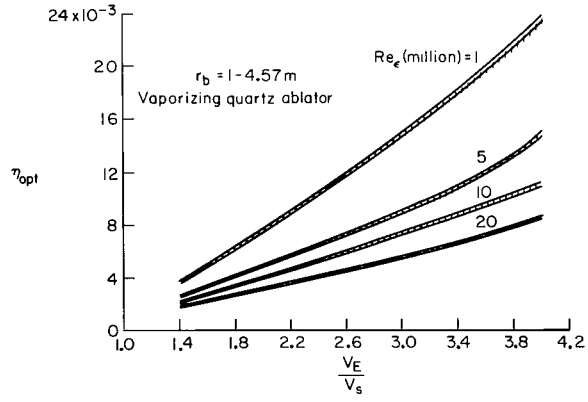

Figure 23.- Effect of Reynolds number on energy fraction for constant Reynolds number trajectories.

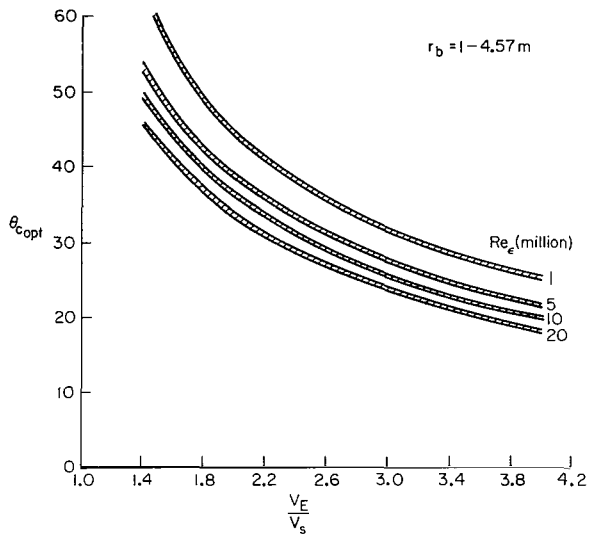

(a) Vaporizing quartz ablator.

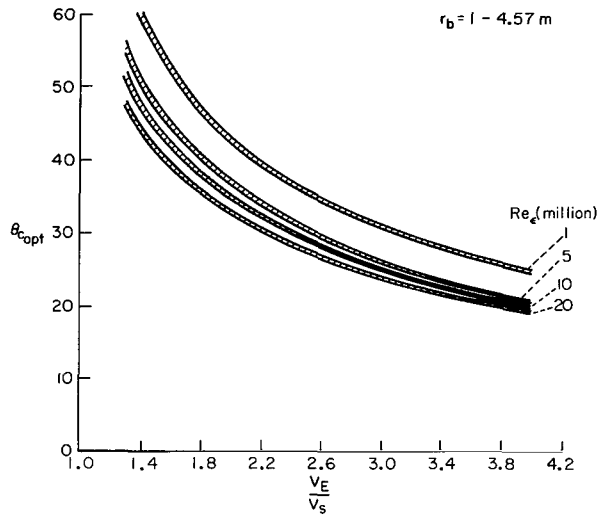

(b) Teflon ablator.

Figure 24.- Optimum cone angles on constant Reynolds number trajectories.

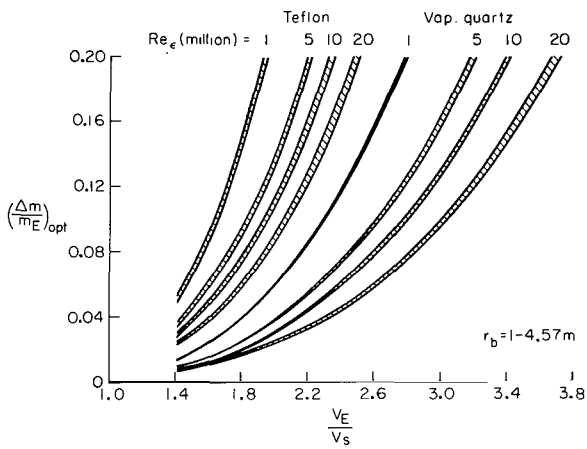

Figure 25.- Mass loss fractions on constant Reynolds number trajectories.

are presented as a function of entry velocity for optimum cones of the two ablation materials.

Comparison of results for constant altitude, constant Reynolds number, and ballistic entry.- The minimum energy fractions calculated for constant altitude entry, constant Reynolds number entry, and ballistic entry are compared in figure 26 for a common Reynolds number limit, 10^7, and a vaporizing quartz ablator. For consistency with the other results, the energy fractions on ballistic entry have been recomputed using the present heat-transfer relations. The constant Reynolds number descent has the lowest heat input, as was expected. For it and the ballistic entry, the energy fractions are insensitive to body size, a consequence of the fact that neither is acceleration limited. For the constant altitude trajectories, the large sensitivity of energy fraction to body size noted earlier appears as a result of the imposed acceleration limit. The energy fractions of the acceleration-limited 1-m base radius bodies are, in fact, off the scale selected and not shown. The constant altitude entry of this size body without an acceleration limit, interestingly enough, falls within the band for ballistic entry. Hence, constant altitude entry without acceleration limit compares almost identically with ballistic entry in respect to total heat input.

The optimum values in the best cases do not differ greatly for the three types of trajectories. It is noteworthy that grazing entries with accelerations within human tolerance can be made in large entry vehicles with heat

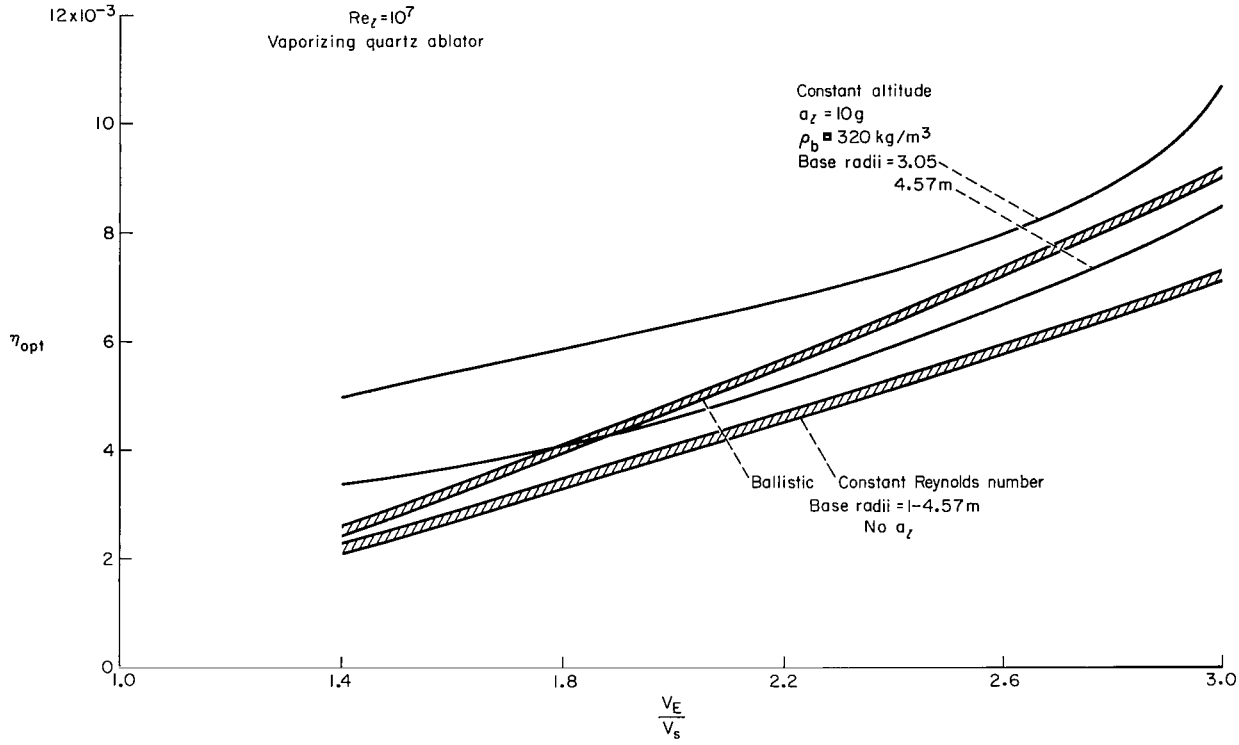

Figure 26.- Comparison of optimum heat input energy fractions for three types of trajectories.

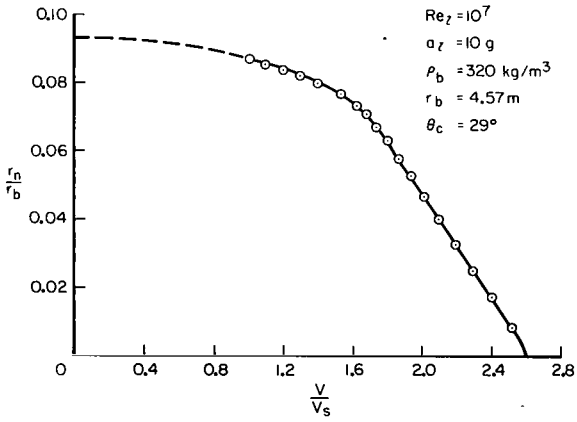

Figure 27.- Nose radius as a function of velocity for a quartz nose on constant altitude entry at $V_E = 2.6\ V_s$.

input energy fractions and mass loss ratios comparable to the lowest possible values obtained on either steep ballistic entry or the optimum, constant Reynolds number descents.

Ablation of the vehicle nose.- The degree to which initially conical entry bodies become blunted by ablation during entry has been calculated for a number of constant altitude and ballistic entries by the method of appendix E. Noses of three materials, Teflon, vaporizing quartz, and graphite, were considered. One example is shown in figure 27, where nose radius to base radius ratio is plotted as a function of velocity for the quartz ablator on constant altitude entry of a 29° cone of an entry velocity of $2.6\ V_s$. The rate of growth of nose radius with velocity, $-dr_n/dV$, is nearly constant from entry down to $V/V_s = 1.8$, after which it diminishes. The calculation is stopped at satellite velocity, at which point the rate of growth is small. Extrapolation to zero velocity gives a radius ratio less than 0.1, corresponding to a mass loss at the tip of the order of 1 percent of the total mass at entry. Furthermore, over 99 percent of the body surface, the bow shock wave is oblique during the period of intense radiative heating

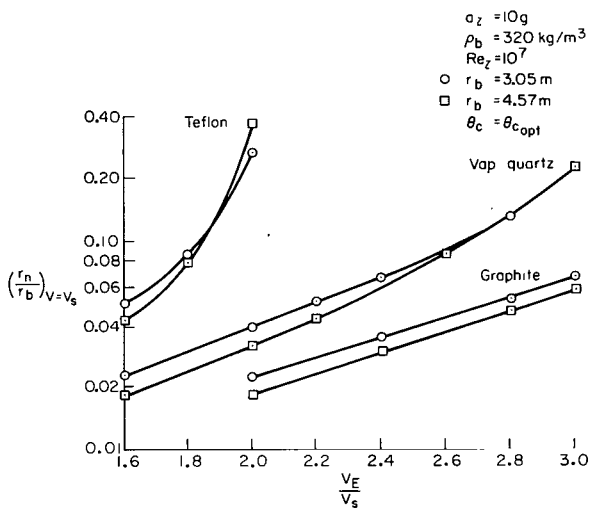

Figure 28.- Nose radius at satellite velocity as a function of entry velocity for initially sharp cones of three materials on constant altitude entry.

so that the radiative heat input is small in the presence of the small nose radius obtained.

Values of the radius ratio at satellite velocity are shown as functions of entry velocity in figure 28 for constant altitude entries with the three tip materials and two body sizes. The final nose radii tend to become very large for Teflon ablators, and moderately large with vaporizing quartz at the higher entry velocities, but remain less than 0.1 r_b for graphite.

For ballistic entry comparable results not calculated previously are shown in figures 29 and 30 for bodies with a base radius of 1 m. The ablation of a Teflon nose for V_E/V_S = 2.0, figure 29, has a history much like that in figure 27. Figure 30, which extends to higher entry velocities than figure 28, shows that on ballistic entry as well as on grazing entry, nose ablation can be severe or moderate, depending on the nose material.

While these estimates should not be regarded as definitive (in view of the assumptions, appendix E), they suggest that optimum conical entry bodies can substantially retain the advantages of pointed cones with respect to

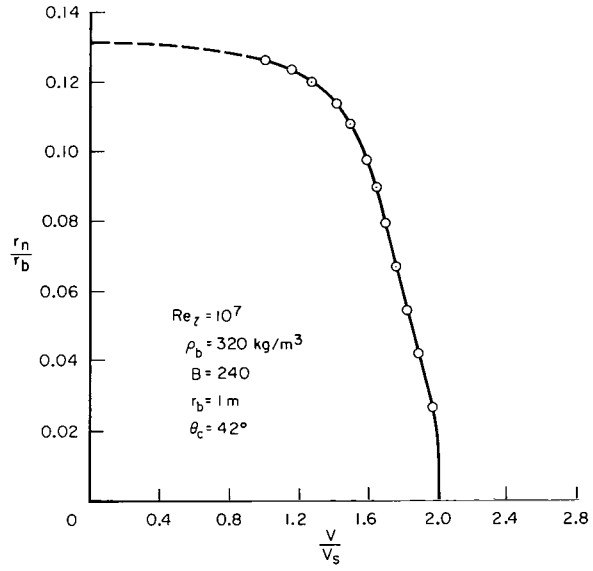

Figure 29.- Nose radius as a function of velocity for a Teflon nose on ballistic entry at an entry velocity of 2 V_s.

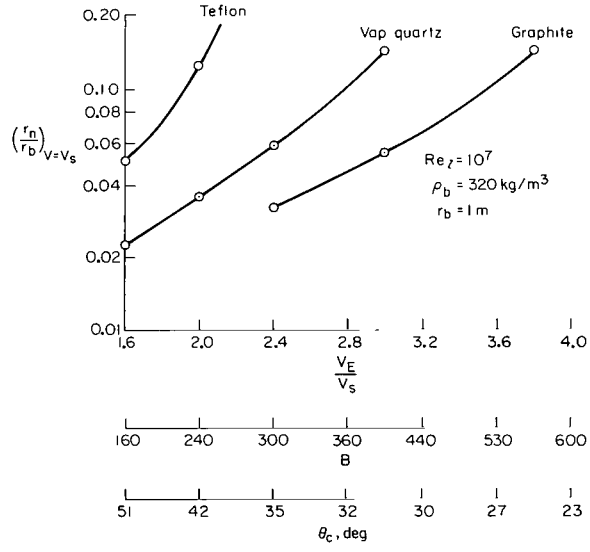

Figure 30.- Nose radius at satellite speed as a function of entry velocity for initially sharp cones on ballistic entry.

radiative heat input,[6] and can have acceptable mass losses at the tip, provided high performance ablation materials, such as the assumed vaporizing quartz and graphite, can be successfully applied.

REVIEW OF ASSUMPTIONS

The present analysis was performed to demonstrate the existence of optimum conditions, to define the magnitude of the optimum heat input, and cone angles, etc., and to identify the effects of the principal variables in parametric fashion. By its nature, such an analysis of a complex problem must be approximate, but the simplifying assumptions made to permit analysis must not invalidate the results to be obtained. To emphasize this, it is useful to review and comment on the assumptions made, which are as follows:

1. The angle between the flight path and the horizontal is small. Comment: Satisfied exactly for constant altitude entry, and very well satisfied on high-speed portions of constant Reynolds number entries.

2. Changes in mass, cone angle, and base radius of the vehicle are small during entry and may be neglected. Comment: The cone angle and base radius changes are indeed small for cases considered. The mass loss integrated over the trajectory is restricted to 0.2 of the mass at entry or less in cases presented.

3. The drag coefficient is constant during entry. Comment: Should be valid in hypersonic speed range for bodies of the class studied.

4. Laminar boundary layer can be maintained by restricting the local Reynolds number below a suitable limit. Comment: Assumption is consistent with knowledge of boundary-layer transition processes for nonablating surfaces at lower speeds. Its validity at the speeds and ablation conditions of this analysis requires experimental study. Considerations of roughness of the ablating surface, uniformity of vapor emission with time and over the surface, etc., may enter.

5. The ratio of the Reynolds number evaluated at boundary-layer edge properties to that evaluated at free-stream properties is a constant for any one angle. Comment: Approximately true, and, as shown in appendix D, the constant chosen will yield a local Reynolds number equal to or less than the selected limit.

6. The density profile of the earth's atmosphere has an exponential dependence on altitude. Comment: Not a critical assumption for this analysis.

---

[6]A favorable effect of tip blunting is to reduce the convective heating rate. The reduction is sizable when the shear layer of the body nose becomes larger than the boundary-layer thickness. This effect has (conservatively) been neglected in the present analysis.

7. The heat-transfer coefficients may be represented by equations given in the text. Comment: Much of the speed range considered is beyond the range of present day laboratory tests. The equations employed are based on presently available theoretical and experimental information, and use best estimates of high-temperature gas properties. For conical flow, less extrapolation of radiative and convective transport properties is required than for stagnation point flow, since the enthalpy is well below stagnation enthalpy. For example, the radiative heating on optimum cones at $V_E/V_S = 3$ is within the range of present day experiments on blunt bodies, and should not be in doubt by more than a factor of 2. With larger cone angles and blunt bodies, larger uncertainty exists in the radiative transfer. For example, the vacuum ultraviolet contribution, recently discovered to be important, has not been included in the formulas presented, and would increase the heat input for $U > 1.4\ V_S$. Convective heating is presently believed to be subject to less uncertainty than the radiative heating in this high-speed range.

8. Flow along streamlines outside the boundary layer may be regarded as isoenergetic, that is, flow energy losses by radiation may be neglected. Comment: The heat-transfer coefficient is defined in terms of the available flow energy. Small values of the radiative heat-transfer coefficient therefore signify essentially constant energy flow and, from the results presented, it is clear that the optimum bodies satisfy the assumption. Nonoptimum bodies, however, may have large values of C_{H_e}, and deviate from isoenergetic flow. Several cases were analyzed allowing for energy loss along streamlines and one is shown in figure 31. The energy input is affected by only a few percent for this 60° half-angle cone. For smaller angle cones, the effect is even less.

9. Radiative reabsorption in the shock layer may be neglected; that is, the shock layer is assumed to be optically thin. Comment: If radiative intensity at all wavelengths is small compared to that of a black body of the shock-layer temperature, the assumption is justified. This appears to be the case for the optimum and near-optimum cones analyzed. For large angled cones with shock-layer temperatures high enough to produce significant ionization, $U > 1.4\ V_S$, the vacuum ultraviolet region of the spectrum becomes important (refs. 16, 17) and reabsorption of radiation may be an important consideration. Other atmospheric gases, notably those generating CN as a radiating species, can also encounter important reabsorption at particular wavelengths. With air, no such predominant radiators are present.

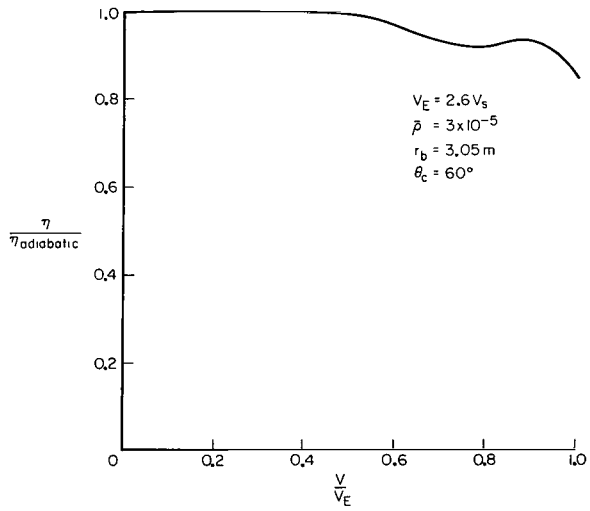

Figure 31.- The effect of a nonadiabatic shock layer on the heating of an effectively sharp cone of $\theta = 60°$ on constant altitude entry.

10. The heat blocking and ablative behavior of the heat shield may be simplified, as represented by equations (9) and (18). Comment: This assumption has four parts. The form assumed for the heat blocking factor ψ has been discussed in the Analysis and Presentation

of Results. Although the magnitude of the heat input is affected by the value assigned to the asymptote σ, the variation of heat input with cone angle is unaffected, and the existence and nature of the optimum do not depend on the value chosen. Second, chemical reactions at the surface and in the boundary layer have been neglected. For the quartz material, this is appropriate, but for graphite and Teflon, some chemical reaction must be expected. However, at the very high speeds considered, reaction products tend to be dissociated at boundary-layer temperatures, and chemical reactions may not be of overriding importance. Third, heat reradiated by the ablation shield is neglected. Comparison of the rate at which heat can be reradiated with the heat input rate shows that the reradiation is small compared to the heat input rate for surface temperatures below about 3500° K. This is near the maximum permissible surface temperature for any material, so the assumption may be allowed. Fourth, the production of ablation vapor is assumed to be a result of convective heating only. For cones of near-optimum angle, this is a good approximation. For cones of larger angle experiencing large radiative heat input, the transpiration rates would be higher than calculated, with a moderate reduction in convective heat input. It is clear that the treatment of the ablation shield is approximate, and that some basic understanding of the high velocity behavior is still lacking, but it should be adequate to indicate the mass loss and the heat blocked to a first approximation.

11. The heating of partial cones, modified to generate lift, may be approximated by analysis of the complete cones from which they are derived. Comment: Intuitively, one can see that this will be the case to a useful order of approximation. In detail, a number of corrections or modifications to the analysis would be required to treat the modified cone. For example, in the case of oblique base plane modification described in appendix C, if the mean base radius of the upper and lower meridians is regarded as the base radius of the analysis, the convective heat input is reduced on the upper meridian and increased on the lower meridian in approximately compensating amounts. The same is true for radiative input. The Reynolds number limit must be applied to the longest (lower) meridian, which decreases the stream density permitted, and is perhaps the main effect. Certainly, the magnitude of the over-all result will not be greatly affected.

12. The heating increment on tangential entry into the atmosphere from the point of entry to the point of joining the selected constant altitude or constant Reynolds number trajectory is equivalent to that obtained by entering the design trajectory at full entry velocity. Comment: For vehicles of the size, density, etc., considered herein, velocity losses of the order of a few percent of V_E will, in actual entries, occur before design altitude is reached. Since the Reynolds numbers are, in this phase, lower than the design value, convective heat input will be increased (eq. (28)), while radiative input will be diminished (eq. (22)). The altitude range of the principal velocity loss is within one atmospheric scale height of the design altitude, so that the convective heat input may be shown to be increased by a factor smaller than $e^{1/2}$. If, in fact, a factor of 2 is allowed on the values of C_H for this interval, the increment in η is typically 0.0002. The approximation is therefore satisfactory.

CONCLUDING REMARKS

The results presented indicate that heat input energy fractions on hyperbolic grazing entries, with acceleration limited to within human tolerance, can be limited to about the same levels as on ballistic entries which have no acceleration limit. Under the best conditions, corresponding to moderately high boundary-layer transition Reynolds numbers, entry may occur at velocities up to 3 V_s with less than 1 percent of the initial kinetic energy finding its way into the body as heat. Corresponding mass losses of the heat shield may be less than 20 percent of the total mass at entry with shield materials of high heat of ablation. Conical bodies away from the optimum, of which blunt bodies may be considered one extreme, will experience heat inputs many times greater than the optimum.

The optimum bodies are generally swept back to such an extent that the radiative heat input is small compared to the convective. An exception to this arises if the local Reynolds number must be limited below one million to maintain laminar boundary layer, in which case the radiative input may comprise the order of one-third the total heat input at optimum. The total heat input is substantially greater in these cases than in the case of higher limit Reynolds numbers.

The determination of the level of Reynolds number for maintaining a laminar boundary layer is an important problem requiring experimental solution. Not only are the heat input and heat-shield mass loss increased for low values of the Reynolds number limit, but the acceleration may be reduced well below its limiting value with the consequence that a high lift-drag ratio is required. At values of entry velocity approaching 3 V_s, the L/D required tends, in any case, toward higher values than can be aerodynamically generated by modification of the optimum cones. Lowering the total acceleration to obtain a low Reynolds number will, at such velocities, usually insure that insufficient aerodynamic lift is available.

For entries into the earth's atmosphere at or below 10 g total acceleration and with levels of L/D which can be generated with cones of optimum half-angle, the maximum entry velocity will be limited to about 3 V_s. Higher velocity entry might be accommodated by use of multiple pass entries or by use of rocket thrust to supply lift or drag force.

The trajectories selected for analysis tend to give near the minimum possible convective heat input by staying near the highest permissible Reynolds number. Trajectories on which the Reynolds number is allowed to go far below this limit will increase the heat input, as will those that go above it and incur a turbulent boundary layer. The constant Reynolds number descent obtains the minimum convective heat input exactly, for a given limit Reynolds number, cone angle, entry velocity, and ablation shield. If on this trajectory the cone angle is selected to make the total heat input a minimum, and if the

radiative input is found to be small, then the entry may be identified as a minimum heat input case with respect to both trajectory and cone angle.

Ames Research Center
National Aeronautics and Space Administration
Moffett Field, Calif., Jan. 7, 1966

APPENDIX A

THE LAMINAR CONVECTIVE HEAT-TRANSFER COEFFICIENT

The problem of laminar convective heat transfer to nonablating cones at very high flight velocities has been investigated theoretically by G. Chapman (ref. 10). Chapman finds that his many solutions for a variety of flight velocities from 4.5 to 25 km/s, cone angles from 15° to 60°, and wall temperatures from 1000° K to 4200° K can be correlated by equations of the form

$$\frac{Nu}{\sqrt{Re_w}} = \frac{F}{V^{0.36}} \tag{A1}$$

where

$$Nu = \frac{q}{h_t - h_w} \frac{c_{p_w} x}{k_w} \tag{A2}$$

$$Re_w = \frac{\rho_w u_e x}{\mu_w} \tag{A3}$$

and q is the local heating rate at a distance x from the cone vertex.[1] The coefficient F is weakly dependent on wall temperature and surface pressure (see fig. 3, ref. 10), and takes the following values when V is in m/s.

	T_w, °K			
p_w, atm	500	1000	3000	4200
0.1	6.86	8.45	9.07	10.11
1.0			9.72	
10.0			9.89	

Equation (A1) may be put in the form of the heat-transfer coefficient used herein if the heat-transfer rates over the surface are integrated and the integral is equated to the present defining equation of total heating rate at zero ablation:

$$C_{H_{c_o}} \frac{\rho V^3 A}{2} = \frac{4}{3} \frac{F}{V^{0.36}} \frac{h_t - h_w}{\sqrt{r_b \sin \theta_c}} \frac{\sqrt{\rho_w \mu_w u_\epsilon}}{Pr_w} A \tag{A4}$$

[1]Some departures from the correlation occur when wall enthalpy approaches recovery enthalpy and when the boundary layer becomes highly ionized. Chapman (ref. 10) discusses the extent of these deviations and the conditions under which they occur. It is sufficient here to note that they do not importantly affect the optimum conditions of the present analysis.

For adiabatic flow $h_t = h + V^2/2$, and furthermore $|h - h_w| \ll V^2/2$, so $h_t - h_w$ may be replaced by $V^2/2$. Hence,

$$C_{H_{c_o}} = \frac{4}{3} \frac{F}{V^{0.86}} \frac{\sqrt{\frac{\rho_w}{\rho} \mu_w \frac{u_\epsilon}{V}}}{\sqrt{\rho r_b \sin \theta_c} \, Pr_w} \tag{A5}$$

In addition, u_ϵ/V may be replaced by $\cos \theta_c$ to a good order of approximation, and

$$\frac{\rho_w}{\rho} = \frac{p_w}{p} \frac{T}{Z_w T_w} = \left[\frac{V^2 \sin^2 \theta_c}{RT} + 1 \right] \frac{T}{Z_w T_w}$$

where the wall pressure ratio is converted to the terms in the bracket by use of Newtonian theory, and $V^2 \sin^2 \theta_c / RT \gg 1$ for the velocities and cone angles considered. Equation (A5) becomes

$$C_{H_{c_o}} = \frac{4}{3} \frac{F V^{0.14}}{\sqrt{\rho r_b}} \frac{\sqrt{\frac{\mu_w}{Z_w R T_w} \sin \theta_c \cos \theta_c}}{Pr_w} \tag{A6}$$

which is of the form of equation (16) with

$$C_c = \frac{4}{3} \frac{F}{\sqrt{2\rho_o}} \frac{\sqrt{\frac{\mu_w}{Z_w R T_w}}}{Pr_w} \tag{A7}$$

From this, it may be seen that C_c depends on surface temperature and pressure, through F and through the air properties at the wall. In neither case is the dependence a strong one, however. For example, $\sqrt{\mu_w/T_w}$ increases by only 27 percent as T_w is lowered from 3000° K to 1000° K, while Z_w remains very close to 1.0. The conditions chosen for evaluating C_c were $T_w = 3000^\circ$ K and p_w in the range from 0.1 to 1.0 atmosphere. With these selections,

$$C_c = 1.16 \times 10^{-4} \left(\frac{s}{m} \right)^{0.14} m^{0.5} \tag{A8}$$

Comparison of equations (16) and (17) with the laminar convective heating equations of reference 5 shows that in the lower speed region of that reference, $V < 13{,}000$ m/s, the given values of $C_{H_{c_o}}$ agree to within about 10 percent. The higher speed equation of reference 5 was based on extrapolation of a lower speed theory, and underestimates the present results by factors ranging from 1.1 at 13,000 m/s to about 4.0 at $V = 30{,}000$ m/s. This fact should be noted in comparing numerical results of reference 5 with the present results.

APPENDIX B

INTEGRATION OF CONVECTIVE HEATING RELATION FOR CONSTANT REYNOLDS NUMBER TRAJECTORIES

For the constant Reynolds number trajectory the laminar convective heat-transfer relation, equation (28), may be integrated in closed form for $j = 1/6$.

$$\eta_c = \frac{C_c \sqrt{\sin 2\theta_c}}{V_E^2 \sqrt{r_b} \sin^2 \theta_c} \int_o^{V_E} \left(\sigma + \frac{1 - \sigma}{1 + K_c V^2} \right) \frac{V^{7/6}\, dV}{\sqrt{\frac{K}{\rho_o V}}} \tag{B1}$$

where, for constant Reynolds number, $\rho V = K$ is constant. The integral may be expressed as a sum of two integrals

$$\eta_c = \frac{C_c \sqrt{\rho_o \sin 2\theta_c}}{V_E^2 \sqrt{K r_b} \sin^2 \theta_c} \left(\int_o^{V_E} \sigma V^{5/3}\, dV + \int_o^{V_E} \frac{1 - \sigma}{1 + K_c V^2} V^{5/3}\, dV \right) \tag{B2}$$

The first integral can be evaluated immediately, while the second requires the change of variable $Y = V^{2/3}$, which results in

$$\eta_c = \frac{C_c \sqrt{\rho_o \sin 2\theta_c}}{V_E^2 \sqrt{K r_b} \sin^2 \theta_c} \left[\frac{3}{8} \sigma V_E^{8/3} + \frac{3(1 - \sigma)}{2} \int_o^{Y_E} \frac{Y^3\, dY}{1 + K_c Y^3} \right] \tag{B3}$$

The solution to this integral can be found in reference 18 and is

$$\eta_c = \frac{C_c \sqrt{\rho_o \sin 2\theta_c}}{V_E^2 \sqrt{K r_b} \sin^2 \theta_c} \left[\frac{3}{8} \sigma V_E^{8/3} + \frac{3(1 - \sigma)}{2} \left(\frac{Y}{K_c} - \frac{1}{6 K_c^{4/3}} \ln \frac{K_c^{2/3} Y^2 + 2 K_c^{1/3} Y + 1}{K_c^{2/3} Y^2 - K_c^{1/3} Y + 1} - \frac{1}{\sqrt{3}\, K_c^{4/3}} \tan^{-1} \frac{\sqrt{3}\, K_c^{1/3} Y}{2 - K_c^{1/3} Y} \right)_o^{Y_E} \right] \tag{B4}$$

After evaluating this expression at the limits of integration and returning to the original variable V, we find

$$\eta_c = \frac{C_c \sqrt{\rho_o \sin 2\theta_c}}{V_E^2 \sqrt{Re\mu} \sin^{5/2} \theta_c} \left\{ \frac{3}{8} \sigma V_E^{8/3} \right.$$

$$+ \frac{3(1 - \sigma)}{2K_c^{4/3}} \left[\left(K_c V_E^2 \right)^{1/3} - \frac{1}{6} \ln \frac{(K_c V_E^2)^{2/3} + 2(K_c V_E^2)^{1/3} + 1}{(K_c V_E^2)^{2/3} - (K_c V_E^2)^{1/3} + 1} \right.$$

$$\left. \left. - \frac{1}{\sqrt{3}} \tan^{-1} \frac{\sqrt{3} (K_c V_E^2)^{1/3}}{2 - (K_c V_E^2)^{1/3}} \right] \right\} \qquad \text{(B5)}$$

where the constant K has been replaced by its definition $\rho V = Re\mu/r_b$.

APPENDIX C

LIFT-DRAG RATIOS OF MODIFIED CONES

Three ways of generating lift with cones are known or have been proposed: (1) controlling attitude of the unmodified cone; (2) removing all or part of the upper conical surface above a given plane surface; and (3) using an oblique base plane. The latter two alternatives are sketched in figure 32.

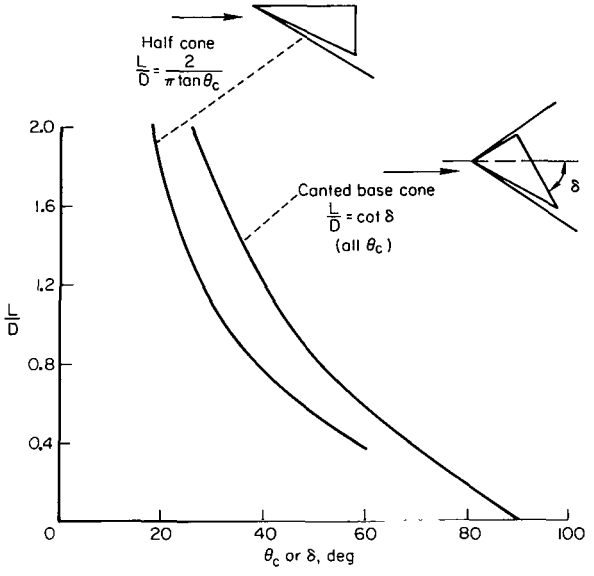

Figure 32.- Lift-drag ratios of modified cones at zero angle of attack.

The first alternative is the least attractive for hyperbolic entry, since it creates crossflow conditions in the boundary layer that are very damaging to laminar stability (see, e.g., refs. 19 and 20). Furthermore, since the effective angle presented by the lower surface to the stream is $\theta_c + \alpha_t$, and since L/D and α_t must diminish with velocity, the effective cone angle and drag coefficient diminish during entry increasing the total heat input. At any speed, C_D is less than its allowable maximum which is dictated by the angle presented on the lower surface only. Hence, this alternative does not recommend itself compared to the other two.

The second alternative, proposed in reference 21, provides the maximum lift-drag ratio in the limiting case of the half cone. That ratio is shown as a function of cone angle in figure 32. Any smaller value of L/D down to zero may be selected by canting the plane of the upper surface at an angle facing the stream. In the absence of skin friction and base drag, this modification gives infinite L/D at $\theta_c = 0$. Cases of present interest, for example, $\theta_c = 30^\circ$, have maximum L/D up to 1.1. Crossflow affects this configuration along the intersection of the plane surface with the conical surface, where a pressure jump exists laterally (in the case of a rounded intersection, distributed to give a lateral pressure gradient). Turbulent boundary layer might be expected to appear first along this region and to spread over the adjoining surfaces at appropriate Reynolds numbers. The convective heating of the upper surface imposes a penalty not considered quantitatively in the analysis. The estimation of the heating of the upper surface poses some theoretical problems in the presence of a blunted tip and the crossflow phenomenon described above.

The third alternative, proposed in reference 22, was investigated by means of Newtonian theory in reference 23, and the results for lift-drag ratio are also shown in figure 32. The lift-drag ratio of the cone with an oblique base plane is the same as for a flat plate inclined at the base angle to the

stream, that is, $L/D = \cot \delta$. As $\delta \rightarrow 0$, L/D becomes very large. However, for bodies enclosing a real physical volume, δ must be greater than θ_c, so that for $\theta_c = 30^\circ$, a base angle of 42° would comprise a very thin and doubtfully practical case, which would have the same L/D as the 30° half cone, namely, 1.1. Bodies of this cone angle with a useful volume arrangement might, in fact, be restricted to lift-drag ratios of 0.8 or less. This modification should, however, be free of crossflow effects, except those occurring behind the vehicle base, and may present the best possibility for retaining laminar flow over the conical heat shield. It is also the closest of the three alternatives to the assumptions of the heating analysis, which treats a pure cone at zero angle of attack.

With alternatives (2) and (3), the method of reducing the component of L/D in the vertical plane as velocity diminishes along the trajectory is to roll the vehicle until L/D times the cosine of the roll angle equals the L/D required. To prevent lateral curvature of the flight path, a roll oscillation symmetrical about the position for vertical lift vector is followed, the amplitude determining the vertically effective component of L/D. The angles of pitch and sideslip of the vehicle are (ideally) zero throughout entry, simplifying the theoretical treatment of heating.

APPENDIX D

DEVELOPMENT OF TRAJECTORY RELATIONS

In this appendix, the first section develops the equations for acceleration-limited, Reynolds number-limited constant altitude flight; the second develops the equations for constant Reynolds number descent; and the third defines the relationship between local and free-stream Reynolds numbers on cones in hypervelocity flight.

EQUATIONS OF CONSTANT ALTITUDE DECELERATION

The lift force required to maintain circular flight above satellite velocity is given by

$$L = [(V/V_s)^2 - 1]W \tag{D1}$$

from which it follows that the lift-to-drag ratio is

$$\frac{L}{D} = \left[\left(\frac{V}{V_s}\right)^2 - 1\right] \frac{W/C_D A}{q_\infty} \tag{D2}$$

For zero dynamic pressure q_∞, L/D is required to be infinite, since the need for the lift force remains, while the drag has gone to zero (note asymptotic behavior of the curves in figure 3). To fully display the effect of velocity on L/D, equation (D2) is written

$$\frac{L}{D} = \frac{(V/V_s)^2 - 1}{(V/V_s)^2} \frac{W/C_D A}{(1/2)\rho V_s^2} \tag{D3}$$

where the factor on the right is a constant for a given vehicle and altitude, and may be identified as the L/D required at infinite velocity with this vehicle and altitude.

The altitude is selected to maintain specified limits on the total acceleration and Reynolds number. The axial acceleration may be written as

$$\frac{a_x}{g} = \frac{(1/2)\rho V_s^2}{W/C_D A} \left(\frac{V}{V_s}\right)^2 \tag{D4}$$

while the component radial to the earth is the centripetal acceleration

$$\frac{a_y}{g} = \frac{V_s^2}{gr} \left(\frac{V}{V_s}\right)^2 = \left(\frac{V}{V_s}\right)^2 \tag{D5}$$

so the total acceleration is

$$\frac{a}{g} = \sqrt{\frac{a_x^2 + a_y^2}{g^2}} = \left(\frac{V}{V_s}\right)^2 \sqrt{\left[\frac{(1/2)\rho V_s^2}{W/C_D A}\right]^2 + 1} \tag{D6}$$

By equation (D3), this may be written entirely in terms of V and L/D.

$$\frac{a}{g} = \sqrt{\left[\frac{\left(\frac{V}{V_s}\right)^2 - 1}{\frac{L}{D}}\right]^2 + \left(\frac{V}{V_s}\right)^4} \tag{D7}$$

which is solved for L/D to yield equation (30) of the text. The maximum value of a/g occurs when $V = V_E$ and, in acceleration limited cases, is set equal to the limit value of acceleration, a_l/g. The L/D varies after entry with velocity according to equation (D3), while the acceleration decays according to equation (D6). The stream density at which the peak acceleration attains the limit value may be obtained from equation (D6).

$$\rho = 2 \frac{W/C_D A}{V_s^2} \sqrt{\frac{(a_l/g)^2}{(V_E/V_s)^4} - 1}$$

$$= \frac{\rho_b r_b g}{3 V_s^2 \sin^2 \theta_c \tan \theta_c} \sqrt{\frac{(a_l/g)^2}{(V_E/V_s)^4} - 1} \tag{D8}$$

If, on the other hand, the altitude is determined by the Reynolds number limit, then at entry onto the constant altitude trajectory, when Reynolds number is maximum,

$$Re_l = \left(\frac{\rho_\epsilon u_\epsilon S}{\mu_\epsilon}\right)_E \tag{D9}$$

where the subscript ϵ identifies fluid properties at the boundary-layer edge and S is the slant length of the cone. As will be shown, to a good order of approximation, in the following equation

$$\frac{\rho_\epsilon u_\epsilon S/\mu_\epsilon}{\rho V r_b/\mu} = \frac{k}{\tan \theta_c} \tag{D10}$$

$k = k(U)$ only. The parameter $k(U)$ has an approximately constant value of 2 for $U \leq V_s$ and diminishes to 1.3 at $U > 1.3\ V_s$. Through equation (D10), equation (D9) may be written in terms of free-stream variables as

$$Re_l = \frac{k}{\tan \theta_c} \left(\frac{\rho V r_b}{\mu}\right)_E \tag{D11}$$

and the free-stream density determined by the Reynolds number limit is

$$\rho = Re_l \frac{\tan \theta_c}{k} \frac{\mu}{V_E r_b} \tag{D12}$$

Thus, with the density for the acceleration limit defined by equation (D8) and for the Reynolds number limit by equation (D12), the value selected to observe both limits is the smaller of the two.

EQUATIONS OF CONSTANT REYNOLDS NUMBER DESCENT

The condition that $\rho_\epsilon u_\epsilon S/\mu_\epsilon$ remain constant along the trajectory requires that $\rho V r_b/\mu$ be approximately constant also. If we assume that variations in the stream viscosity with altitude may be neglected, and that r_b is not appreciably diminished by ablation in flight, then by equation (D10)

$$\rho V = Re_\epsilon \frac{\tan \theta_c}{k} \frac{\mu}{r_b} = \text{constant} = K \tag{D13}$$

and equation (5) which, for small path angle γ, governs deceleration along the trajectory becomes

$$\frac{1}{V} \frac{dV}{dt} = - \frac{C_D A}{m} \frac{K}{2} \tag{D14}$$

so that

$$\frac{V}{V_E} = e^{- \frac{C_D A}{m} \frac{K}{2} t} \tag{D15}$$

Similarly, in terms of x as independent variable,

$$\frac{dV}{dx} = - \frac{C_D A}{m} \frac{K}{2} \tag{D16}$$

and

$$V = V_E - \frac{C_D A}{m} \frac{K}{2} x \tag{D17}$$

The rate of descent through the atmosphere implicit in equations (D13), (D15), and (D17) may be obtained as follows. Assume, following reference 1, that

$$\frac{\rho}{\rho_o} = e^{-\beta y} \tag{D18}$$

By (D13) and (D18),

$$\rho_o e^{-\beta y} V = K \tag{D19}$$

Eliminating V between (D15) and (D19) gives

$$\frac{K}{\rho_o V_E} e^{\beta y} e^{\frac{C_D A}{m} \frac{K}{2} t} = 1 \tag{D20}$$

or

$$\beta y + \frac{C_D A}{m} \frac{K}{2} t = \ln \frac{\rho_o V_E}{K} = \ln \frac{\rho_o V_E}{\rho V} \tag{D21}$$

Equation (D21) shows that the rate of descent is steady, as can be made clear by taking the derivative to obtain

$$V_y = -\frac{dy}{dt} = \frac{C_D A}{m} \frac{K}{2\beta} \tag{D22}$$

The flight-path angle is obtained as a function of the velocity from

$$\sin \gamma = \frac{V_y}{V} = \frac{C_D A}{m} \frac{K}{2\beta V} \tag{D23}$$

and may also be obtained as a function of t or x by use of (D15) or (D17).

The lift-to-drag ratio required to follow this path and the accelerations experienced may be derived as follows. The motion is not circular about the center of the planet, and to find L/D, we must consider the actual flight-path curvature. The notation employed is indicated in sketch (b). About the instantaneous center of curvature

$$R\, d\gamma' = dx \tag{D24}$$

The angle γ' is measured relative to the reference direction C-1, while the local flight-path angle γ is referred to the local tangent to the planet's surface. From the sketch

$$d\gamma' = d\gamma + d\xi \tag{D25}$$

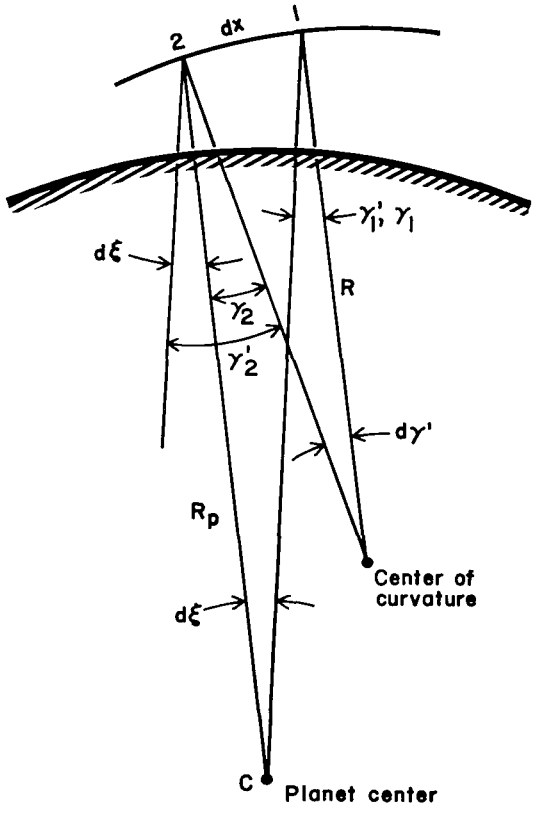

Sketch (b)

Since $d\xi$ is a differential, we may write

$$R_p \, d\xi = (dx)\cos \gamma \tag{D26}$$

which is combined with (D24) and (D25) and solved for R to obtain

$$R = \frac{1}{(d\gamma/dx) + [(\cos \gamma)/R_p]} \tag{D27}$$

By Newton's second law of motion

$$W \cos \gamma + L = mV^2 \left(\frac{d\gamma}{dx} + \frac{\cos \gamma}{R_p} \right) \tag{D28}$$

from which, noting that $gR_p = V_s^2$,

$$\frac{L}{W} = \left(\frac{V}{V_s} \right)^2 \left(R_p \frac{d\gamma}{dx} + \cos \gamma \right) - \cos \gamma \tag{D29}$$

By equations (D23) and (D17)

$$\sin \gamma = \frac{C_D A}{m} \frac{K/2\beta}{V_E - (C_D A/m)(K/2)x} \tag{D30}$$

and by differentiation of (D30)

$$\frac{d\gamma}{dx} = \beta \sin \gamma \tan \gamma \tag{D31}$$

so (D29) may be written for the constant Reynolds number descent

$$\frac{L}{W} = \left(\frac{V}{V_s} \right)^2 \left(\beta R_p \sin \gamma \tan \gamma + \cos \gamma \right) - \cos \gamma \tag{D32}$$

By the definition of drag coefficient

$$\frac{D}{W} = \frac{C_D A}{W} \frac{1}{2} \rho V^2 = \frac{C_D A}{W} \frac{K}{2} V \tag{D33}$$

and L/D is obtained by dividing (D32) by (D33):

$$\frac{L}{D} = \frac{[(V/V_s)^2 - 1]\cos \gamma + (V/V_s)^2 \beta R_p \sin \gamma \tan \gamma}{(C_D A/W)(KV_s/2)(V/V_s)} \tag{D34}$$

For small γ, $\cos\gamma = 1$, $\sin\gamma = \tan\gamma = V_y/V$, and we may write

$$\frac{L}{D} = \frac{W}{C_D A}\frac{2}{KV_s}\frac{V_s}{V}\left[\left(\frac{V}{V_s}\right)^2 - 1 + \beta R_p\left(\frac{V_y}{V_s}\right)^2\right] \tag{D35}$$

With $V_y = 0$, this reduces to the expression for constant altitude flight, equation (D2). With nonzero V_y, a further reduction is accomplished by relating the factor outside the bracket to V_y/V through equation (D23).

$$\frac{L}{D} = \frac{1 - (V_s/V)^2}{\beta R_p V_y/V} + \frac{V_y}{V} \tag{D36}$$

Thus, the L/D required is obtained as a function of velocity and descent rate, while the descent rate has a known dependence on the vehicle parameters and the constant Reynolds number selected.

The axial acceleration is given by equation (D4). The transverse acceleration for small γ is, by (D27), (D28), and (D31),

$$\frac{a_y}{g} = \beta R_p\left(\frac{V_y}{V_s}\right)^2 + \left(\frac{V}{V_s}\right)^2 \tag{D37}$$

which may be compared with equation (D5). The total acceleration is given by

$$\frac{a}{g} = \left(\frac{V}{V_s}\right)^2\sqrt{\left[\frac{KV_s}{2(V/V_s)(W/C_D A)}\right]^2 + \left[\beta R_p\left(\frac{V_y}{V}\right)^2 + 1\right]^2} \tag{D38}$$

RELATIONSHIP BETWEEN LOCAL AND FREE-STREAM REYNOLDS NUMBER

The ratio of the local Reynolds number based on edge properties and slant length to the free-stream Reynolds number, referred to base radius, may be written

$$\frac{Re_\epsilon}{Re} = \frac{\rho_\epsilon u_\epsilon \mu S}{\rho V \mu_\epsilon r_b} \tag{D39}$$

For a thin hypersonic shock layer

$$\frac{u_\epsilon}{V} \doteq \cos\theta_c$$

and from the cone geometry, $S/r_b = 1/\sin\theta_c$. Furthermore,

$$\rho_\epsilon = \frac{p_\epsilon}{RT_\epsilon Z_\epsilon} \doteq \frac{\rho(V\sin\theta_c)^2}{RT_\epsilon Z_\epsilon}$$

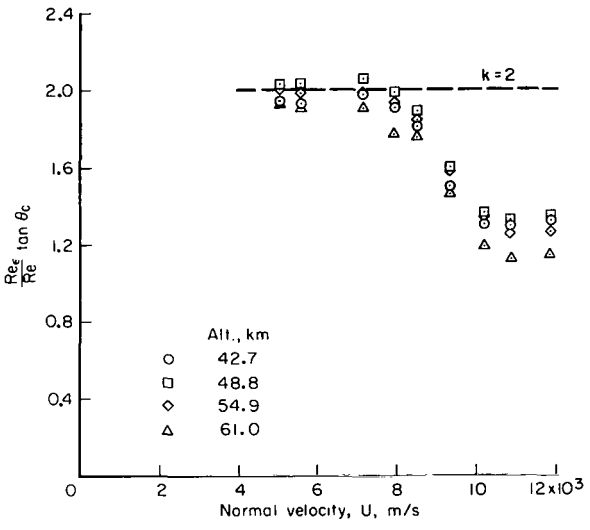

Figure 33.- Ratio of local to free-stream Reynolds number for cones in hypervelocity flight.

so equation (D39) becomes

$$\frac{Re_\epsilon}{Re} = \frac{(V \sin \theta_c)^2}{RT_\epsilon Z_\epsilon} \frac{\mu}{\mu_\epsilon} \frac{\cos \theta_c}{\sin \theta_c} \qquad (D40)$$

In figure 33, the ratio $(Re_\epsilon/Re)\tan \theta_c$ is plotted as a function of normal velocity component, $V \sin \theta_c$, over the range from 5 to 12 km/s for altitudes ranging from 42.7 to 61 km. The thermodynamic properties were evaluated with the aid of reference 24, and reference 25 was used for the transport properties.

The flight conditions shown in figure 33 are representative of those for near-optimum bodies. If Reynolds number ratio is written as

$$\frac{Re_\epsilon}{Re} \tan \theta_c = k \qquad (D41)$$

then, $k \doteq 2$ for normal velocities from 5 to 8 km/s and decreases to about 1.3 at $U = 10$ km/s. In order to be conservative, and for convenience, $k = 2$ has been used throughout the analysis. Use of this value of k at the higher values of U has the effect that for a given value of Re, Re_ϵ is less than the limit Reynolds number which is being imposed.

APPENDIX E

ANALYSIS OF NOSE ABLATION

The heating rate per unit area at the stagnation point of a blunted nose may be written

$$\frac{dH_{st}}{dt} = C_{H_{st}} \frac{1}{2} \rho V^3 \tag{E1}$$

where $C_{H_{st}}$ is the dimensionless local stagnation-point heat-transfer coefficient consisting of a laminar convective and a radiative component. The convective component may be written, based on theoretical results given in reference 26, as

$$C_{H_{st_c}} = (3.65 \times 10^{-4} / \sqrt{\rho r_n}) \psi \tag{E2}$$

where the constant 3.65×10^{-4} has the dimensions $(kg/m^2)^{1/2}$, and ψ represents the reduction in heating due to transpiration and is assumed to be given by equation (18).

The radiative component may be written, assuming the shock layer is optically and physically thin,

$$C_{H_{st_e}} = C_e \delta V^{q-3} \frac{\rho^{p-1}}{\rho_o^{p}} \tag{E3}$$

where C_e is given in the text and δ is the shock-wave standoff distance at the stagnation point, given for spherical noses (ref. 27) by

$$\delta = 0.78 \, r_n \frac{\rho}{\rho_2} \tag{E4}$$

Here, ρ_2 is the gas density behind the shock wave, and is, for equilibrium shock layers, a function of ρ and V only. The heat-transfer coefficient

$$C_{H_{st}} = C_{H_{st_c}} + C_{H_{st_e}} \tag{E5}$$

is thus a function of ambient density, velocity, and nose radius. The rate of mass loss at the stagnation point may be written

$$\frac{\dot{m}}{A} = \frac{dH_{st}/dt}{\zeta} \tag{E6}$$

and the rate of surface regression is

$$\dot{x}_n = \frac{\dot{m}}{A\rho_b} \tag{E7}$$

so that, by (E6) and (E1),

$$\dot{x}_n = \frac{C_{H_{st}} \frac{1}{2} \rho V^3}{\zeta \rho_b} \tag{E8}$$

The following assumptions are now made: (1) The nose is originally a sphere segment of small finite radius and remains spherical during ablation. (2) Deviations of the heat transfer from that given by the above relations, due to deviations from chemical and thermodynamic equilibrium, are small. (3) Energy release and surface erosion due to chemical reactions of the ablation materials with atmospheric gases may be neglected. (4) No material is removed by spallation.

Under the assumption of spherical blunting, the rate of increase in nose radius may be related to the rate of surface regression at the stagnation point

$$\dot{r}_n = \dot{x}_n \frac{\sin \theta_c}{1 - \sin \theta_c} \tag{E9}$$

so that

$$\dot{r}_n = \frac{C_{H_{st}} \frac{1}{2} \rho V^3}{\zeta \rho_b} \frac{\sin \theta_c}{1 - \sin \theta_c} \tag{E10}$$

Given the trajectory relations, which define the variations of ρ and V with time, and the heat-transfer coefficient, equations (E2) through (E5), equation (E10) may be numerically integrated to obtain the nose radius as a function of time during entry.

REFERENCES

1. Allen, H. Julian; and Eggers, A. J., Jr.: A Study of the Motion and Aerodynamic Heating of Ballistic Missiles Entering the Earth's Atmosphere at High Supersonic Speeds. NACA Rep. 1381, 1958.

2. Page, William A.: Shock-Layer Radiation of Blunt Bodies Traveling at Lunar Return Entry Velocities. Inst. Aerospace Sci., Annual Meeting, New York, Jan. 21-23, 1963, IAS Paper 63-41.

3. Seiff, Alvin; Goodwin, Glen; and Wick, Bradford H.: Effect of Vehicle Configuration on Combined Heating Loads With Special Reference to Radiative Heating. NASA-Industry Apollo Tech. Conf., Washington, D. C., July 1961.

4. Allen, H. Julian: Gas Dynamics Problems of Space Vehicles. NASA-University Conf. on the Science and Technology of Space Exploration, Chicago, Illinois, Nov. 1-3, 1962. NASA SP 11, vol. 2, 1962.

5. Allen, H. Julian; Seiff, Alvin; and Winovich, Warren: Aerodynamic Heating of Conical Entry Vehicles at Speeds in Excess of Earth Parabolic Speed. NASA TR R-185, 1963.

6. Compton, Dale L.; and Cooper, David M.: Measurement of Radiative Heating on Sharp Cones. AIAA J., vol. 3, no. 1, 1965, pp. 107-114.

7. Seiff, Alvin: Atmosphere Entry Problems of Manned Interplanetary Flight. AIAA-NASA Conf. on Engineering Problems of Manned Interplanetary Exploration, Palo Alto, Calif., Sept. 30-Oct. 1, 1963, AIAA Proc., 1963, pp. 19-33.

8. Seiff, Alvin: Developments in Entry Vehicle Technology. AIAA Annual Meeting, Washington, D. C., June 29-July 2, 1964, AIAA Paper 64-528.

9. Tauber, Michael E.; and Seiff, Alvin: Optimization Analysis of Conical Bodies Making Lifting Hyperbolic Entries Into the Atmospheres of Earth and Mars. AIAA, Entry Tech. Conf., Williamsburg and Hampton, Virginia, Oct. 12-14, 1964, AIAA Pub. CP-9.

10. Chapman, Gary T.: Theoretical Laminar Convective Heat Transfer and Boundary-Layer Characteristics on Cones at Speeds to 24 Km/Sec. NASA TN D-2463, 1964.

11. Adams, M. C.: Recent Advances in Ablation. ARS J., vol. 29, no. 9, Sept. 1959, pp. 625-632.

12. Vojvodich, Nick S.; and Pope, Ronald B.: The Influence of Ablation on Stagnation Region Convective Heating for Dissociated and Partially Ionized Boundary-Layer Flows. 1965 Heat Transfer and Fluid Mech. Inst., Univ. of Calif., Los Angeles, Calif., June 21-23, 1965, Andrew F. Charwat et al., eds., Stanford Univ. Press, 1965, pp. 114-137.

13. Kratsch, K. M.; Hearne, L. F.; and McChesney, H. R.: Theory for the Thermophysical Performance of Charring Organic Heat Shield Composites. LMSC 803099, Lockheed Missiles and Space Co., Oct. 1963.

14. Goldsmith, Alexander; Waterman, Thomas E.; and Hirschhorn, Harry J.: Handbook of Thermophysical Properties of Solid Materials. Vol. I. Macmillan Co., New York, 1961.

15. Chapman, Dean R.; and Kapphahn, Arline K.: Table of Z Functions for Atmosphere Entry Analyses. NASA TR R-106, 1961.

16. Nardone, M. C.; Breene, R. G.; Feldin, S. S.; and Riethof, T. R.: Radiance of Species in High Temperature Air. Rep. R 63SD3, General Electric Co., June 1963.

17. Hahne, Gerhard E.: The Vacuum Ultraviolet Radiation From N^+- and O^+-Electron Recombination in High Temperature Air. NASA TN D-2794, 1965.

18. Petit Bois, G.: Tables of Indefinite Integrals. Dover Pub., Inc., New York, 1961.

19. Seiff, Alvin; and Wilkins, Max E.: Experimental Investigation of a Hypersonic Glider Configuration at a Mach Number of 6 and at Full-Scale Reynolds Numbers. NASA TN D-341, 1961.

20. Chapman, Gary T.: Some Effects of Leading-Edge Sweep on Boundary-Layer Transition at Supersonic Speeds. NASA TN D-1075, 1961.

21. Eggers, Alfred J., Jr.: The Possibility of a Safe Landing. Chap. 13 of Space Technology, Howard S. Seifert, ed., John Wiley and Sons, New York, 1959, 53 pp.

22. Shapland, D. J.: Preliminary Design of a Mars-Mission Earth Reentry Module. Rep. 4-57-64-3, Lockheed Missiles and Space Co., March 1964.

23. Mayo, Edward E.; Lamb, Robert H.; and Romere, Paul O.: Newtonian Aerodynamics for Blunted Raked-Off Circular Cones and Raked-Off Elliptic Cones. NASA TN D-2624, 1965.

24. Moeckel, W. E.; and Weston, Kenneth C.: Composition and Thermodynamic Properties of Air in Chemical Equilibrium. NACA TN 4265, 1958.

25. Hansen, C. Frederick: Approximations for the Thermodynamic and Transport Properties of High-Temperature Air. NACA TN 4150, 1958.

26. Howe, John T.; and Viegas, John R.: Solutions of the Ionized Radiating Shock Layer, Including Reabsorption and Foreign Species Effects, and Stagnation Region Heat Transfer. NASA TR R-159, 1963.

27. Seiff, Alvin: Recent Information on Hypersonic Flow Fields. NASA-University Conf. on the Science and Technology of Space Exploration, Chicago, Illinois, Nov. 1-3, 1962. NASA SP 11, vol. 2, 1962.

NASA-Langley, 1966 A-915

"The aeronautical and space activities of the United States shall be conducted so as to contribute . . . to the expansion of human knowledge of phenomena in the atmosphere and space. The Administration shall provide for the widest practicable and appropriate dissemination of information concerning its activities and the results thereof."

—NATIONAL AERONAUTICS AND SPACE ACT OF 1958

NASA SCIENTIFIC AND TECHNICAL PUBLICATIONS

TECHNICAL REPORTS: Scientific and technical information considered important, complete, and a lasting contribution to existing knowledge.

TECHNICAL NOTES: Information less broad in scope but nevertheless of importance as a contribution to existing knowledge.

TECHNICAL MEMORANDUMS: Information receiving limited distribution because of preliminary data, security classification, or other reasons.

CONTRACTOR REPORTS: Technical information generated in connection with a NASA contract or grant and released under NASA auspices.

TECHNICAL TRANSLATIONS: Information published in a foreign language considered to merit NASA distribution in English.

TECHNICAL REPRINTS: Information derived from NASA activities and initially published in the form of journal articles.

SPECIAL PUBLICATIONS: Information derived from or of value to NASA activities but not necessarily reporting the results of individual NASA-programmed scientific efforts. Publications include conference proceedings, monographs, data compilations, handbooks, sourcebooks, and special bibliographies.

Details on the availability of these publications may be obtained from:

SCIENTIFIC AND TECHNICAL INFORMATION DIVISION

NATIONAL AERONAUTICS AND SPACE ADMINISTRATION

Washington, D.C. 20546